

Intrinsic Absorption Lines in Seyfert 1 Galaxies.

I. Ultraviolet Spectra from the Hubble Space Telescope¹

D. Michael Crenshaw^{2,3}, Steven B. Kraemer², Albert Boggess^{4,5},
Stephen P. Maran^{5,6}, Richard F. Mushotzky⁷, and Chi-Chao Wu⁸

Received 1998 September 22; accepted 1998 November 11

To appear in *The Astrophysical Journal*

¹Based on observations made with the NASA/ESA Hubble Space Telescope, obtained from the data archive at the Space Telescope Science Institute. STScI is operated by the Association of Universities for Research in Astronomy, Inc. under the NASA contract NAS5-26555.

²Catholic University of America and Laboratory for Astronomy and Solar Physics, NASA's Goddard Space Flight Center, Code 681 Greenbelt, MD 20771.

³Email: crenshaw@buckeye.gsfc.nasa.gov.

⁴2420 Balsam Drive, Boulder, CO 80304.

⁵NASA's Goddard High Resolution Spectrograph (GHRS) Investigation Definition Team.

⁶Space Sciences Directorate, Code 600, NASA's Goddard Space Flight Center, Greenbelt, MD 20771.

⁷Laboratory for High Energy Astrophysics, Code 662, NASA's Goddard Space Flight Center, Greenbelt, MD 20771.

⁸Computer Sciences Corporation, Space Telescope Science Institute, 3700 San Martin Drive, Baltimore, MD 21218.

ABSTRACT

We present a study of the intrinsic absorption lines in the ultraviolet spectra of Seyfert 1 galaxies. The study is based on spectra from the *Hubble Space Telescope*, and includes the Seyfert 1 galaxies observed with the Faint Object Spectrograph and Goddard High Resolution Spectrograph at spectral resolutions of $\lambda/\Delta\lambda \approx 1000 - 20,000$ with good signal-to-noise ratios. We find that the fraction of Seyfert 1 galaxies that show intrinsic absorption associated with their active nuclei is more than one-half (10/17), which is much higher than previous estimates (3 – 10%) based on *IUE* data. There is a one-to-one correspondence between Seyferts that show intrinsic UV absorption and X-ray “warm absorbers”, indicating that these two phenomena are related. Although our sample is not complete, we conclude that intrinsic absorption represents an important component that needs to be integrated into our overall physical picture of active galaxies.

The intrinsic UV absorption is generally characterized by high-ionization: C IV and N V are seen in all 10 Seyferts with detected absorption (in addition to La), whereas Si IV is present in only four of these Seyferts, and Mg II absorption is only detected in NGC 4151. The absorption lines are blueshifted (or in a few cases at rest) with respect to the narrow emission lines, indicating that the absorbing gas is undergoing net radial outflow. At high resolution, the absorption often splits into distinct kinematic components that show a wide range in widths (20 – 400 km s⁻¹ FWHM), indicating macroscopic motions (e.g., radial velocity subcomponents or turbulence) within a component. The strong absorption components have cores that are much deeper than the continuum flux levels, indicating that the regions responsible for these components lie completely outside of the broad emission-line regions.

Additional information on the covering factors and column densities can be derived from the absorption profiles in the high resolution spectra. The covering factor of the absorbing gas in the line of sight, relative to the total underlying emission, is $C_{los} \geq 0.86$, on average. The global covering factor, which is the fraction of emission intercepted by the absorber averaged over all lines of sight, is $C_{global} \geq 0.5$. Thus, structures covering large solid angles as seen by the central continuum source (e.g., spherical shells, sheets, or cones with large opening angles) are required. The individual absorption components show a wide range in C IV column densities ($0.1 - 14 \times 10^{14} \text{ cm}^{-2}$), and the ratio of N V to C IV column density varies significantly from one absorption component to the next, even in the same Seyfert galaxy. Thus, the intrinsic absorption in a Seyfert 1 galaxy is typically comprised of distinct kinematic components that are characterized by a range in physical conditions (e.g., ionization parameter and hydrogen column density).

Finally, we show evidence for extreme variability in the intrinsic absorption lines of NGC 3783. In addition to our earlier report of the appearance of a C IV absorption doublet at -560 km s^{-1} (relative to the emission lines) over 11 months, we have detected the appearance of another C IV doublet at -1420 km s^{-1} over 15 months. On the other hand, the C IV absorption lines of NGC 3516 and NGC 4151 were very stable over periods of 6 months and 4 years, respectively. Monitoring observations of individual Seyferts at higher time resolution are needed to distinguish between different sources of variability (variable ionization, motion of gas across the line of sight) and to determine the densities and radial locations of the absorption components.

Subject headings: galaxies: Seyfert – ultraviolet: galaxies

1. Introduction

Seyfert galaxies were originally recognized as a special class of objects from their strong emission lines (Seyfert 1943), and were later subdivided into two groups based on the widths of their emission lines in optical spectra (Khachikian & Weedman 1971). Seyfert 1 galaxies have broad permitted lines with widths $\geq 1000 \text{ km s}^{-1}$ (FWHM), and narrow permitted and forbidden lines with widths $\approx 500 \text{ km s}^{-1}$ (FWHM), whereas Seyfert 2 galaxies show only the narrow emission lines. In turn, these objects are recognized as belonging to the category of objects known as active galaxies (Osterbrock 1984). It has been known for some time that Seyfert galaxies are strong emitters over the entire electromagnetic spectrum (Weedman 1977). The optical continua of Seyfert 1 galaxies are dominated by nonstellar emission that can be characterized by a power-law, as first demonstrated by Oke & Sargent (1968), whereas this component appears to be much weaker in Seyfert 2 galaxies (Koski 1978). These trends extend to the lines and continua observed in the ultraviolet (Wu, Boggess, & Gull 1983) by the *International Ultraviolet Explorer* (*IUE*).

Seyfert (1943) recognized the presence of absorption lines in several of his objects, which he attributed to a “G-type spectrum”. In fact, most of the absorption features in the *optical* spectra of both types of Seyfert can be attributed to stellar features from the host galaxy (Koski 1978; Crenshaw & Peterson 1985). Oke & Sargent (1968) first reported a possible nonstellar absorption feature in the spectrum of NGC 4151; they explain that this feature was first discovered and attributed to He I $\lambda 3889$ self-absorption by O.C. Wilson. Anderson & Kraft (1969) resolved the metastable He I absorption into three components, and discovered hydrogen Balmer ($\text{H}\beta$, $\text{H}\gamma$) absorption corresponding to these components. The components are all blue-shifted relative to the emission lines by up to -970 km s^{-1} , and the authors attributed the blue-shifts to ejection of matter from the nucleus of NGC 4151. Cromwell and Weymann (1970) showed that the strengths of the Balmer absorption lines

are variable, and can occasionally disappear altogether. Anderson (1974) found evidence that the Balmer absorption lines in NGC 4151 can vary on time scales as small as \sim 30 days, and claimed that the absorption and continuum variations are correlated. Anderson also suggested that the absorption region lies outside of the broad emission-line region, because the depth of the $\text{H}\alpha$ absorption was greater than the flux in the nearby continuum.

In the ultraviolet, early observations of NGC 4151, primarily by *IUE*, revealed a rich assortment of intrinsic absorption lines spanning a wide range in ionization from Mg II to N V, as well as fine-structure and metastable absorption lines such as C III* λ 1175 (Davidson & Hartig 1978; Boksenberg et al. 1978; Penston et al. 1981; Bromage et al. 1985). Bromage et al. suggested that the absorption-line variations in NGC 4151 are due to changes in the column densities, rather than the velocity spread of the clouds. In addition, they suggested that the absorbing region is likely to be composed of optically thin gas located outside of the broad emission-line region. Ulrich (1988) described other Seyfert galaxies that show obvious intrinsic absorption in *IUE* spectra. Most of these objects show C IV and N V absorption (along with $\text{L}\alpha$ in most cases), indicating high ionization. Only two Seyferts showed strong evidence for intrinsic Mg II absorption (NGC 4151 and MCG 8-11-11). The absorption features are blue-shifted by as much as -2500 km s^{-1} with respect to the emission lines.

From a large set of *IUE* observations, Ulrich (1988) estimated that only 3 – 10% of all Seyfert 1 galaxies show intrinsic UV absorption. This would suggest that while intrinsic UV absorption is an interesting curiosity, it might not have a strong impact on our understanding of active galaxies. However, only very strong absorption lines (with equivalent widths $> 1 \text{ \AA}$) are detectable at the low spectral resolution ($\lambda/\Delta\lambda = 200 - 400$) and low signal-to-noise ratio ($\text{SNR} < 10$) of the *IUE* spectra. From an examination of a small sample of *HST* spectra, we found that more than half (5/8) of the Seyfert 1

galaxies showed intrinsic C IV absorption (Crenshaw 1997). This indication that intrinsic UV absorption is much more common than previously believed was a principal motivation for expanding our sample of *HST* spectra, as described in this paper.

Another motivation for this study was to investigate the relationship between the UV absorber and the X-ray “warm absorber”, which is characterized by O VII and O VIII absorption edges and is present in about half of the Seyfert 1 galaxies observed in X-rays (Reynolds 1997; George et al. 1998b). Evidence for this highly ionized gas in the line-of-sight to an active galaxy was first reported by Halpern (1984), using the *Einstein Observatory*. Subsequent X-ray satellites provided supporting evidence for warm absorbers, and detailed analysis and modeling of many individual objects were made possible by *ASCA*. Warm absorbers are typically characterized by ionization parameters in the range $U = 0.1 - 10$, temperatures on the order of 10^5 K, and ionized hydrogen column densities in the range $10^{21} - 10^{23}$ cm $^{-2}$ (Reynolds & Fabian 1995; George et al. 1998b).

A connection between the UV and X-ray absorbers was made by Mathur et al. (1994), based on quasi-simultaneous *ROSAT* and *HST* observations of the quasar 3C 351. Using photoionization models, these authors found that a single component of ionized gas could produce both the observed strengths of the O VII and O VIII absorption edges and the equivalent widths of the intrinsic UV absorption lines (O VI $\lambda\lambda$ 1031.9, 1037.6; N V $\lambda\lambda$ 1238.8, 1242.8; C IV $\lambda\lambda$ 1548.2, 1550.8). In these models, most of the carbon, nitrogen, and oxygen are in higher ionization states than those represented by the UV lines. These authors claim that the UV and X-ray absorbers are also the same in 3C 212 (Mathur 1994) and the Seyfert 1 galaxy NGC 5548 (Mathur et al. 1995). However, in some objects, it appears that multiple components characterized by a wide range in ionization parameter and hydrogen column density are needed to explain the wide range in ionization species; such is the case for NGC 3516 (Kriss et al. 1996a; Crenshaw et al. 1998) and NGC 4151

(Kriss et al. 1995). To further investigate the proposition that a single component is responsible for both the UV and X-ray absorption, we felt that it was important to study the absorption in other sources, particularly those with both *HST* and *ASCA* spectra.

Finally, we were motivated by the fact that the intrinsic UV absorption in Seyfert galaxies is qualitatively similar to the “associated” absorption seen in QSOs, in that the lines are relatively narrow ($\leq 300 \text{ km s}^{-1}$), usually close to the emission-line redshift, and in some cases, variable (Hamann 1997; Hamann et al. 1997). The relationship between these relatively narrow absorption systems and the broad absorption lines (BALS), which can exhibit troughs reaching blueshifts as high as $\sim 0.1c$, and are found in approximately 10% of all QSOs (Weymann et al. 1981; Weymann et al. 1991), is not known. The fact that these systems represent high-ionization gas flowing outward from the nucleus suggests that these phenomena may be related. Thus, detailed studies of the intrinsic absorption in Seyfert 1 galaxies should lead to a better understanding of outflows in active galaxies as a function of luminosity. Eventually, we hope that these studies will provide clues to the physical structure of active galaxies, and the relationship between the various absorption, emission, and continuum components in these objects.

To gain a better understanding of the intrinsic absorption in Seyfert 1 galaxies, we have obtained all of the UV spectra of these objects from the *HST* data archive. In this paper, we present new results on the basic properties of the intrinsic UV absorber, its connection to the X-ray warm absorber, its frequency of occurrence in Seyfert 1 galaxies, its global covering factor (relative to the continuum source and broad emission-line region), and its variability. We give a brief history of previous ultraviolet observations of each object in Appendix A, and discuss a few interesting objects that did not satisfy our selection criteria in Appendix B.

2. Observations and Data Reduction

Our original sample was a collection of eight Seyfert 1 galaxies observed under the GHRS GTO (Guaranteed Time Observations) programs of Boggess and Maran; preliminary results on detection of intrinsic absorption were reported in Crenshaw (1997). Results on a few observations from our sample were previously reported for Mrk 509 (Crenshaw, Boggess, & Wu 1993), NGC 3783 (Maran et al. 1996), and NGC 3516 (Crenshaw, Maran, & Mushotzky 1998).

To increase the sample, we searched the *HST* Data Archive to find all of the objects that were identified as Seyfert galaxies by the original proposers and have ultraviolet spectra obtained by the Faint Object Spectrograph (FOS) or the Goddard High Resolution Spectrograph (GHRS). Our search was conducted one year after the removal of these two instruments from *HST* (in 1997 February), so all of the data were nonproprietary and available for retrieval. We did not include the few spectra obtained with the Faint Object Camera (FOC), as they do not satisfy the criteria given below. We included only those objects in this group that have been identified as Seyfert 1, Seyfert 1.5, or narrow-line Seyfert 1 galaxies (Osterbrock & Pogge 1985) in the literature or in the NASA/IPAC Extragalactic Database (NED); hereafter, we refer to this group in a general way as Seyfert 1 galaxies. We excluded Seyfert 2 galaxies or those objects identified as Seyfert 1.8 or 1.9 galaxies (cf., Osterbrock 1981). The reason for excluding these objects is a practical one: it is difficult to detect the absorption lines if they are not seen against strong and relatively broad emission lines and/or strong UV continua. We identified \sim 40 Seyfert 1 galaxies with UV spectra in the archives.

After retrieving and inspecting the UV spectra, we used the following additional criteria for including objects in our survey:

- 1) There must be at least one spectral region in which an intrinsic absorption line might be

detected. In practice, we included objects that had an observation of the redshifted N V, Si IV, C IV, or Mg II emission-line profiles, since the strongest absorption lines come from these species and are embedded in these profiles (Ulrich 1988). We did not include objects that were only observed in the $\text{L}\alpha$ region, since this absorption line can originate in the low-redshift $\text{L}\alpha$ forest (cf., Stocke et al. 1995; Shull et al. 1996).

- 2) The resolution must be sufficient to detect and, in most cases, separate the absorption doublets. In practice, we required that $\lambda/\Delta\lambda$ must be ≥ 1000 , where λ is the observed central wavelength and $\Delta\lambda$ is a resolution element. Henceforth, we refer to FOS spectra with $\lambda/\Delta\lambda \approx 1000$ and GHRS spectra with $\lambda/\Delta\lambda \approx 2000$ as the “low resolution spectra”, and GHRS spectra with $\lambda/\Delta\lambda \approx 20,000$ as the “high resolution spectra”.
- 3) The signal-to-noise ratio (SNR) per resolution element near the expected location of absorption must be ≥ 20 for the low resolution spectra, and ≥ 8 for the high resolution spectra. The detection limit for absorption lines varies according to the SNR; a typical 3σ detection limit (in equivalent width) is $\sim 0.1 \text{ \AA}$ for the low resolution spectra, and $\sim 0.03 \text{ \AA}$ for the high resolution spectra.

We found that 17 Seyfert 1 galaxies in the *HST* data archive satisfied the above criteria. Only a few of the rejected spectra did not satisfy criteria 1 or 2; most of them were rejected on the basis of poor SNR. We emphasize that the observations in our sample were acquired by various investigators for a variety of purposes, and that we did not include QSOs at low redshifts. Thus, our sample is obviously *not* a complete one. In Appendix B, we list those Seyferts that did not satisfy our criteria but show possible evidence for intrinsic absorption.

Table 1 lists the low and high resolution observations for the 17 Seyfert 1 galaxies in our sample. Note that each object has coverage of the redshifted $\text{L}\alpha$, N V, Si IV, and C IV lines, whereas 15 objects have coverage of the redshifted Mg II region (NGC 3783 and II Zw 136 do not have coverage of this region). Spectra that were taken within days of each

other have been averaged to increase the SNR. There are multiple epochs of observation for a number of these objects, although each observation does not necessarily contain every wavelength interval. High resolution observations are available for five Seyfert 1 galaxies observed at low resolution. For these observations, we list the redshifted emission-line profiles that are present in each wavelength setting, where we expect to find the intrinsic absorption lines.

We used the following data reduction procedures for the spectra in Table 1. For the FOS spectra, we retrieved the calibrated files from the *HST* data archive to obtain the wavelength, absolute flux, error flag, and photon noise vectors for each spectrum. For the GHRS spectra, we reduced the raw data using the IDL procedures written for the GHRS Instrument Definition Team (Blackwell et al. 1993); in the process, we determined an average background across the diode array and subtracted it from the gross spectrum for each readout, as described in Crenshaw et al. (1998). We interpolated all of the spectra to a linear wavelength scale, retaining the original approximate wavelength intervals (in Å per bin), and, for each object, we averaged all of the spectra obtained at a particular wavelength setting and within a few days of each other. We then combined spectra that were obtained at different wavelength settings and observed within days of each other at a single point in the wavelength region of overlap. In the few instances where the fluxes did not agree to within 5% in the region of overlap, the longer wavelength spectrum was scaled in flux to match the shorter wavelength spectrum. Thus, we have a final UV spectrum for each entry in Table 1.

In each spectrum, we identified lines that arise in the interstellar medium or halo of our Galaxy using the lists of UV resonance lines in Morton, York, & Jenkins (1988). Those lines that could not be identified as Galactic in origin were considered to be candidates for intrinsic absorption. Specifically, absorption lines with heliocentric velocities greater

than a few hundred km s^{-1} , at the proper wavelength separations for the doublets, and with equivalent widths ≥ 3 times the measurement errors (see below) were considered to be intrinsic. In addition, only $\text{L}\alpha$ lines that occurred at radial velocities close to those of other detected lines were considered to be intrinsic, since those at other velocities could be due to the low-redshift $\text{L}\alpha$ forest.

Figures 1 and 2 present the far-UV (1200 – 1700 Å) portion of the low resolution spectra. The locations of the strongest Galactic absorption lines (Morton et al. 1988) are also shown. Figure 1 shows the seven Seyfert 1 galaxies that did not show detectable intrinsic absorption. Figure 2 shows the ten Seyfert 1 galaxies with intrinsic $\text{L}\alpha$, $\text{N V } \lambda\lambda 1238.8, 1242.8$, $\text{Si IV } \lambda\lambda 1393.8, 1402.9$, and/or $\text{C IV } \lambda\lambda 1548.2, 1550.8$ absorption lines. Note that the intrinsic absorption lines span a large range in equivalent width and velocity width, and tend to occur in the cores of the emission-line profiles or are blueshifted with respect to the emission lines. In a few cases, multiple velocity components can be seen, even at this relatively low resolution.

Figures 3 and 4 give the high-resolution spectra of Seyfert 1 galaxies with intrinsic absorption. Figure 3 shows the C IV region in four Seyferts, and demonstrates the necessity of high spectral resolution for resolving absorption components. Figure 4 shows the corresponding $\text{L}\alpha$ and N V components, when available.

3. Direct measurements

We used the following procedures to measure the intrinsic absorption lines that we detected. To determine the shape of the underlying emission, we fit a cubic spline to regions on either side of the absorption. For those cases in which the absorption occurs in the very core of the line, this procedure may underestimate the underlying emission if there is a

significant narrow-line contribution that has not been properly taken into account. Based on visual inspection of the unabsorbed profiles in the same spectrum (e.g., C III] $\lambda 1909$), we do not expect this to be a serious problem. To normalize the absorption profiles, we divided the observed spectra by the cubic spline fits. We then made direct measurements of the centroid, equivalent width (EW), and full-width at half-maximum (FWHM) of each visually distinct absorption component. Obviously, the number of visible components may depend on spectral resolution, so we consider the low and high resolution spectra separately. We note that our distinction between components and structure within components is somewhat subjective.

We determined the uncertainties in the centroids and FWHMs of each feature from different reasonable fits to the emission on either side of the absorption lines. We determined uncertainties in EWs from the sum in quadrature of the error in fitting the underlying emission and the uncertainty due to photon noise. Finally, we excluded from further consideration any absorption feature with an EW less than three times its uncertainty.

3.1. Detection of intrinsic absorption

Table 2 provides information on the redshifts of Seyfert 1 galaxies in our sample; 4 of these 17 objects are generally regarded as narrow-line Seyfert 1 galaxies, as noted. Redshifts from H I observations (when available) and from the narrow optical emission lines (primarily [O III] $\lambda\lambda 4959, 5007$) were obtained from NED. The H I redshifts are probably more indicative of the systemic velocities of the host galaxies, but we have values for only eight galaxies. The optical redshifts tend to be slightly lower, on average, but within ~ 100 km s^{-1} of the neutral hydrogen redshifts. To be consistent, we adopt the optical redshifts when determining the radial velocities of the absorption lines relative to the Seyfert galaxy, with the understanding that the absorption velocities relative to the systemic redshift are

likely to be within 100 km s^{-1} of these values. We note that in a few cases, the absorption lines in Figure 2 appear to be slightly redshifted with respect to the cores of the broad emission lines (e.g., in Mrk 509), due to a slight blueshift of the high ionization emission lines with respect to the lower ionization lines (see Gaskell 1982).

In Table 2, we specify whether or not each Seyfert 1 galaxy shows intrinsic UV absorption, based on our criteria and according to the detection limits that we gave in the previous section. The Seyferts with intrinsic C IV absorption always show N V and $\text{Ly}\alpha$ absorption at the same approximate velocities, as we discuss in more detail later. We also specify whether or not each Seyfert 1 galaxy shows evidence for an X-ray warm absorber (Reynolds 1997; George et al. 1998b). This table confirms our earlier finding that intrinsic UV absorption is very common: more than half (10/17) of the Seyfert 1 galaxies show intrinsic absorption lines.

3.2. Results from the direct measurements

Tables 3 and 4 present direct measurements of the intrinsic absorption lines in the low and high resolution spectra, respectively. We give the observed centroid (λ_{obs}), the equivalent width (EW), our identification, and the radial velocity, relative to the optical redshift, for each absorption feature. Where there is evidence for more than one kinematic component, we number each component beginning with the one at the shortest observed wavelength. In a few instances, an intrinsic absorption component is blended with another Galactic or intrinsic line; in these cases, we identify the contributors and give the centroid for the entire feature, but do not give other direct measurements. For the high resolution spectra in Table 4, we also give the full-width at half-maximum (FWHM) of each component, when possible, since the absorption features are resolved (the instrumental FWHM is $\sim 15 \text{ km s}^{-1}$). Some components are blended enough to prevent an accurate

measure of their widths.

Measurement errors for λ_{obs} are typically $0.05 - 0.1 \text{ \AA}$ ($10 - 20 \text{ km s}^{-1}$) for the low resolution spectra and 0.02 \AA ($\sim 4 \text{ km s}^{-1}$) for the high resolution spectra; measurement errors for FWHM are typically $\sim 10 \text{ km s}^{-1}$. We provide more realistic uncertainties in v_r and FWHM below, by comparing values for all of the ions associated with each kinematic component.

We summarize the kinematic components that we have detected in Tables 5 and 6. The radial velocity centroids and FWHM are averages from all of the lines that we think are associated with one kinematic component, and the uncertainties are standard deviations of the averages. As we noted earlier, the number of components is highly dependent on the spectral resolution. For objects that have both high and low resolution spectra, it is clear that the low resolution values are just “averages” for blends of the strongest lines. In Mrk 509, there is an offset in v_r between the low and high resolution spectra of $\sim 80 \text{ km s}^{-1}$, which is probably due to a zero-point error in the low resolution wavelength scale of $\sim 0.3 \text{ \AA}$. Similar errors in v_r are possible for the other low resolution spectra.

3.3. Conclusions based on direct measurements

We can draw some important conclusions from Tables 2, 5, and 6 and Figures 2 – 4, to support and extend previous results on the intrinsic UV absorption lines (which were based on a few Seyfert 1 galaxies, see section 1):

1. From the low resolution sample, the frequency of occurrence of intrinsic absorption is $f = 10/17 = 0.59$. When intrinsic absorption is detected, high ionization lines (C IV, N V) and $\text{Ly}\alpha$ are always seen. The intermediate ionization line of Si IV is seen in only 4/17 of the Seyfert 1 galaxies. Of the 15 objects with near-UV coverage, only NGC 4151 shows

evidence for low-ionization (Mg II) absorption,

2. The centroids of the absorption lines are blueshifted by up to -2100 km s^{-1} , or occasionally at rest, with respect to the narrow emission lines (and relative to neutral hydrogen, when it is detected). Thus, the UV absorbers are, for the most part, undergoing radial outflow with respect to the nuclei of these Seyfert 1 galaxies.

3. At high resolution, the absorption lines often split into distinct kinematic components. The components are resolved, and exhibit a range of widths (20 – 400 km s^{-1} FWHM). Most of the components have widths much larger than that expected for thermally stable photoionized gas, even if they arise in the warm absorber (FWHM of C IV $\approx 20 \text{ km s}^{-1}$ at 10^5 K). This indicates macroscopic motions within a component, such as turbulence or the superposition of additional radial velocity components.

4. Lines that are narrow and within a few hundred km s^{-1} of the systemic radial velocity could potentially come from the interstellar medium or halo of the host galaxy. However, most of the intrinsic absorption lines arise close to the nucleus, because they are broad, have large blueshifts, and/or they are variable (see section 5).

5. In the high resolution spectra, the cores of the strongest absorption components are deeper than the heights (in flux) of the continua. This indicates that both the central continuum source and at least a portion of the BLR is occulted by the UV absorber. When we know the size of the BLR (e.g., from reverberation mapping experiments), we can determine lower limits to the size of the absorber in the plane of the sky and its distance from the continuum source (see section 4.3).

6. From Table 3, we can see that there is a one-to-one correspondence between those Seyferts that show UV and X-ray absorption in this sample; six objects show both UV and X-ray absorption, and two objects show neither (although the case for a warm absorber in

NGC 7469 is not strong). Thus, although the sample is small, it appears that there is a connection between the UV and X-ray warm absorbers; however, this does not require that they arise from the same zone, characterized by a single ionization parameter.

4. Absorption profiles

Additional information can be derived from the resolved absorption lines in the high resolution spectra. We have omitted the low resolution spectra from this analysis for the following reasons. 1) The absorption lines seen at low resolution are often comprised of multiple kinematic components, and these components are likely to be characterized by different physical conditions. 2) It is more difficult to determine the intrinsic shapes of the underlying profiles in the low resolution spectra, since the absorption components are broadened and blended. 3) Many of the absorption lines are saturated in the low resolution spectra, which typically leads to underestimates of the column densities ⁹.

4.1. Covering factors

The methods we used to analyze the absorption profiles follow those of Hamann et al. (1997). We consider the case where the region responsible for an absorption component

⁹Lower limits to the column densities of the absorption lines in the low resolution spectra can be calculated directly from the EWs in Table 3, by assuming the case of unsaturated lines (Spitzer 1978). Other techniques for estimating the column densities from unresolved or marginally resolved absorption lines include the curve-of-growth method (Spitzer 1978), and the apparent optical depth method (Savage & Sembach 1991). These techniques are based on simplifying assumptions, which are discussed in these references.

does not completely cover the emission source(s) behind it. If this effect is present and not corrected for, the column densities will be underestimated. We define the covering factor, C_{los} , to be the fraction of continuum plus BLR that is occulted by the absorber in our line of sight. We will consider the case where the covering factor could differ from one kinematic component to the next (but not within a component, as discussed below). If we normalize the absorption lines by dividing by the underlying emission, and I_r is the residual flux in the core of the absorption line at a particular radial velocity, then we can determine a lower limit to the covering factor in the line of sight from the residual flux:

$$C_{los} \geq 1 - I_r. \quad (1)$$

We can also determine a lower limit to the fraction of BLR flux that is occulted by the absorber:

$$C_{los}^{BLR} \geq \frac{1 - I_c - I_r}{1 - I_c}, \quad (2)$$

where I_c is the fraction of the underlying emission at a particular radial velocity due to the central continuum source.

The actual value of C_{los} for a component can be determined from a doublet, if both lines of the doublet are unblended with other lines (Hamann et al. 1997). If the expected ratio of the optical depths of the doublet is 2 (as for C IV and N V), then

$$C_{los} = \frac{I_1^2 - 2I_1 + 1}{I_2 - 2I_1 + 1}, \quad (3)$$

where I_1 and I_2 are the residual fluxes in the cores of the weaker line (e.g., C IV $\lambda 1550.8$) and stronger line (e.g., C IV $\lambda 1548.2$), respectively.

A lower limit to C_{los} is easily obtained, particularly if the absorption components are resolved. To determine a well-constrained value of C_{los} , however, we need both members of the doublet to be clean (unblended with other lines), reasonably strong lines, high

SNR, and an accurate estimate of the underlying emission. In addition, since even the strong components are affected by blending with other components in their wings, we are constrained to determining C_{los} in the cores of these components.

In practice, we determined the covering factor for a few (2 – 5) resolution elements across the core of each component, and then calculated the average and uncertainty. Actual values of the covering factors, as opposed to lower limits, were determined only for a few strong, unblended components (see Figures 3 and 4). For the lower limits, we chose those lines that yield the highest values for that component (implicitly assuming that for a given kinematic component, the covering factor is the same for $\text{L}\alpha$, C IV, and N V).

Table 6, gives C_{los} and C_{los}^{BLR} for each kinematic component in the high resolution spectra, along with the line used to determine these values. We note that when actual values are determined, they are close to unity (except for NGC 3783).

4.2. Column densities

Since the absorption components are resolved, we can determine the column density of each component from its optical depth as a function of radial velocity (v_r). If the covering factor $C_{los} = 1$ for a component, then the optical depth at a particular v_r is given by:

$$\tau = \ln \left(\frac{1}{I_r} \right), \quad (4)$$

If $C_{los} \neq 1$, then the optical depth at a particular radial velocity is:

$$\tau = \ln \left(\frac{C_{los}}{I_r + C_{los} - 1} \right) \quad (5)$$

(Hamann et al. 1997). In principal, C_{los} can be a function of radial velocity (v_r), but we have assumed that it is constant for a given component.

The column density is then obtained by integrating the optical depth across the profile:

$$N = \frac{m_e c}{\pi e^2 f \lambda} \int \tau(v_r) dv_r \quad (6)$$

(Savage & Sembach 1991), where f is the oscillator strength and λ is the laboratory wavelength (Morton et al. 1988).

In Table 7, we give the column densities for each component in the high resolution spectra, for the case of $C_{los} = 1$. The values are averages of those from each member of the doublet, if unblended with other components; otherwise they are from the line that is least affected by blending. Horizontal lines in the table indicate that the component was not detected at that epoch. The column densities in Table 7 are larger than those derived by assuming unsaturated lines by as much as factor of ~ 3 , due to the substantial optical depths in many of the components (e.g., see Crenshaw et al. 1998).

To illustrate the effects of partial covering on the measurements, Table 7 also gives column densities for the few instances that we could actually determine reliable C_{los} values. The greatest effect is seen for NGC 3783, where a covering factor of ~ 0.5 leads to an increase in the column density by a factor of ~ 2 . We also note that if the optical depths are high, even a covering factor close to one can, if not corrected for, have a significant effect on the column densities. For example, $C_{los} = 0.99$ and 0.98 for components 1 and 2 in NGC 3516, respectively, but the effects on the measured column densities are still significant due to the large optical depths. In this particular case, we have suggested that the measured covering factors are not unity because of grating-scattered light, which occurs at the 1 – 2% level (Crenshaw et al. 1998). Grating-scattered light is almost certainly present at this level in all of the GHRS spectra presented here.

We have only a few column densities for the case in which C_{los} has been derived. Thus, for the purpose of discussion, we will refer to the column densities derived from $C_{los} = 1$, with the understanding that the true column densities may be underestimated by a factor

of ~ 2 or less.

4.3. Conclusions from the absorption profiles

In addition to the effects that the covering factors have on column density measurements, we can use them to place important constraints on the absorption regions. Table 6 shows that C_{los}^{BLR} is always positive, indicating that at least a portion of the BLR is occulted by each component. This result alone does not provide a tight constraint, because the absorber could be closer to the continuum source than the BLR, and still intercept a fraction of the emission from the far side of the BLR. However, we note that there is at least one component in each object with $C_{los}^{BLR} \geq 0.9$, except for NGC 3783. Thus, in four of the five Seyfert 1 galaxies in Table 6, there is at least one component of the absorbing gas that essentially covers the BLR (or at least the high-ionization portion characterized by C IV and N V emission). Since the sizes of the C IV emitting regions in these objects are a few light days (Wanders et al. 1997, and references therein), the absorption regions responsible for these components must be greater than a few light days from the continuum source, and greater than a few light days in extent (in the plane of the sky).

We define C_{global} to be the fraction of the underlying emission that the intrinsic UV absorber (as a whole) covers, averaged over all lines of sight for all Seyfert 1 galaxies. Thus,

$$C_{global} = \langle C_{los} \rangle f, \quad (7)$$

where f is the fraction of Seyfert 1 galaxies that show intrinsic absorption, which we have determined to be 0.59 for our sample. For any Seyfert 1 galaxy, C_{los} for the ensemble of absorption components must be greater than or equal to the largest value for any single component. We take the average of the largest values or lower limits of C_{los} from each Seyfert, and find $\langle C_{los} \rangle \geq 0.86$, which leads to $C_{global} \geq 0.51$. We note that these values

are estimates, and may be affected by the small sample size, as well as biases on the part of the observers who selected these Seyfert galaxies.

Thus, as an ensemble, the regions responsible for the UV absorption typically cover *at least* half of the sky as seen by the central continuum source. To illustrate this result, we take two extremes: 1) the covering factor could be close to one-half in all Seyfert 1 galaxies, or 2) the covering factor could be one in the Seyferts with observed absorption and the absorbing gas is not present in the other Seyferts. Obviously, the true situation could be somewhere in between. In either case, C_{global} provides an important geometric constraint for the intrinsic absorber. For example, geometries such as spherical shells, large pieces of shells or sheets, or cones with large opening angles are favored.

Finally, we discuss the column densities in Table 7. We concentrate on the values determined for $C_{los} = 1$ (with the understanding that they may be slight underestimates of the true column densities). There is a substantial range in the column densities of the components, from 0.1 to $14 \times 10^{14} \text{ cm}^{-2}$ (the former value is at our detection limit). By comparison, the column density of C IV is much higher in a typical BLR cloud: $N(\text{C IV}) \geq 10^{18} \text{ cm}^{-2}$ (Ferland & Mushotzky 1982; Ferland et al. 1992).

As we mentioned previously, it is difficult to accomodate the larger values of the C IV column density ($\sim 10^{15} \text{ cm}^{-2}$) in X-ray “warm absorber” models that are characterized by a single ionization parameter. In addition, we note that in the case of NGC 5548, where multiple components of N V absorption have been measured, the ratio of $N(\text{N V})/N(\text{C IV})$ varies substantially, ranging from 2.1 to 18.2. This is strong evidence that the ionization parameter varies significantly from one kinematic component to the next. Combined with the evidence that Si IV absorption is present in some objects and absent in others, and the detection of Mg II absorption and other low ionization lines in only one object (NGC 4151), these results indicate that there is a wide range in physical properties, particularly ionization

parameter, among UV absorbers in different Seyferts and among different components in the same Seyfert.

5. Variability

To investigate the variability of the intrinsic UV absorption in our sample, we concentrate on the high resolution spectra, since it is difficult to determine accurate column densities in the low resolution data. As in the past, when absorption variations are detected, they are found in the column densities of the lines and not in the radial velocities. We are limited to the three Seyfert 1 galaxies with multiple epoch observations at high resolution: NGC 3516, NGC 3783, and NGC 4151. (Variability studies of other objects with other satellites are described in Appendix A.)

NGC 3783 shows extreme variability in its C IV absorption lines (Figure 3). There is no evidence for absorption in the GHRS spectrum on 1993 February 5, but a C IV absorption doublet is present 11 months later (on 1994 January 6) at -560 km s^{-1} (relative to the optical emission). After a subsequent interval of 15 months (on 1995 April 15), an additional C IV doublet is evident at a radial velocity of -1420 km s^{-1} (there was no significant change in the column density of the other component). We reported the first variation in Maran et al. (1996), and the second in Crenshaw et al. (1997); in Table 7, we give the magnitude of these variations in terms of the derived column densities. We also note that the single spectrum of the N V region on 1993 February 21 (Figure 4) was obtained just 16 days after the first C IV spectrum, which showed no absorption. Since C IV and N V are always present together in our low-resolution spectra, this *suggests* (but does not prove) that the absorption varied rapidly over this 16 day interval.

As reported in Crenshaw et al. (1998), we detected no variability in the C IV

absorption components of NGC 3516 over a 6-month period, although changes in the column density at the $\leq 25\%$ level cannot be ruled out, due to the fact that the lines are saturated. In this case, we know that previous variations of the C IV absorption were due to a broad, blue-shifted component that disappeared between 1989 October and 1993 February (Koratkar et al. 1996). For NGC 4151, Weymann et al. (1997) found that the C IV absorption was constant over a 4-year period, with the exception of one transient event. We note that over the time span of the HST observations, the lines of C IV and N V in these two Seyferts were saturated, and therefore modest ($\sim 25\%$) variations in the column densities of these high-ionization lines would not be detected. In NGC 4151, variations in weaker (and lower ionization) absorption lines have been detected with *HUT* and *ORFEUS*, as described in Appendix A.

There are two likely sources of absorption variations: 1) changes in the ionization fractions due to continuum variations, and/or 2) changes in the total column of gas (e.g., due to bulk motion across the line-of-sight). The former could be identified from a correlation between continuum and absorption variations, but obviously we do not have enough observations of NGC 3783, closely spaced in time, to establish such a correlation. The best case for a correlation between continuum and absorption variations has been established for the neutral hydrogen absorption and low-ionization lines of NGC 4151 (Kriss et al. 1996c; Espey et al. 1998).

The best case for bulk motion as a source of variability is the aforementioned disappearance of the broad, blueshifted absorption component of C IV in NGC 3516. This component has not reappeared in recent observations, despite substantial continuum variations, which suggests that the absorbing gas has moved out of the line-of-sight. Assuming tangential velocities comparable to the largest observed radial velocities, an absorber could move across the BLR on a time scale of months to years (Maran et al.

1996). It is possible that both continuum variability and bulk motion are responsible for absorption variability, and that they could very well be occurring on different time scales.

If variations in column density can be attributed to changes in the ionizing continuum, then monitoring observations can be used to probe the physical conditions in the gas. The time lag between continuum and absorption variations will provide the recombination and/or ionization time scales, and thus the electron density (n_e) and/or radial location (r) of the gas, respectively (Shields & Hamann 1997; Krolik & Kriss 1997). With only one of these quantities (n_e or r), the other can be determined with the assistance of photoionization models, which provide the ionization parameter and ionic ratios from the observed column densities of different ions. For example, Shields & Hamann (1997) used our first detection of variability in NGC 3783 to derive lower limits to the electron density ($n_e \geq 300 \text{ cm}^{-3}$) and upper limits to the distance of the absorbing gas from the central continuum source ($r \leq 10 \text{ pc}$). Other examples are given in Appendix A, but in every case, only an upper limit has been determined for the time lag between continuum and absorption variations, which leads to a lower limit on the density and an upper limit on the radial distance.

6. Summary

We have presented the first systematic study of intrinsic absorption in active galaxies that is based on ultraviolet spectra from *HST*. Although the sample is not complete and subject to biases on the part of the observers that selected these objects, we find that intrinsic absorption is much more common than previously believed (Ulrich 1988), occurring in more than half (10/17) of the Seyfert 1 galaxies in this study. The absorption is due to highly ionized gas that is flowing outward from the nucleus. At high resolution ($\lambda/\Delta\lambda \approx 20,000$) the absorption often breaks up into multiple kinematic components, which are likely characterized by different physical conditions, and probably different distances from

the nucleus.

We have shown that at least some of the absorption components arise from regions that are completely outside of the BLR, and that these regions must be at least a few light days in size (in the plane of the sky) to occult the BLR. As an ensemble, the intrinsic absorbers cover a large part of the sky ($\geq 50\%$) as seen from the continuum source. We note that these values

The absorption components in our sample remain stable in radial velocity over at least several years, but, in one case, show extreme variations in column density over one year. Previous studies have suffered from a lack of spectral or temporal resolution, but indicate that the UV absorber lies between the BLR and NLR (except for narrow components near the systemic velocity of the host galaxy that may arise from that galaxy's halo.) Intensive monitoring observations (e.g, with *HST*) are needed produce well-sampled continuum and absorption light curves, in order to explore the range of physical characteristics of the absorbing gas, determine its origin, and explore its relation to the X-ray warm absorber.

Eight Seyfert 1 galaxies in this study have high-quality *HST* and *ASCA* spectra, and there is a one-to-one correspondence between those objects that show intrinsic UV absorption and those that show X-ray warm absorbers. Thus these two phenomena are related, but additional studies are needed to determine the exact nature of their relationship. Specifically, detailed photoionization calculations are needed to match the observed column densities, and thereby test the need for multi-zone models. We will address this issue in a companion paper.

This research has made use of the NASA/IPAC Extragalactic Database (NED) which is operated by the Jet Propulsion Laboratory, California Institute of Technology, under contract with the National Aeronautics and Space Administration. This research has also

made use of NASA's Astrophysics Data System Abstract Service. D.M.C. and S.B.K. acknowledge support from NASA grant NAG 5-4103. Support for this work was provided by NASA through grant number AR-08011.01-96A from the Space Telescope Science Institute, which is operated by the Association of Universities for Research in Astronomy, Inc., under NASA contract NAS5-26555.

A. Notes on individual Seyfert 1 galaxies in the sample

A.1. WPVS 007 (WPV85 007)

This relatively unknown narrow-line Seyfert 1 shows variable and ultrasoft X-ray emission (Grupe et al. 1995); no information is available on the possibility of an X-ray warm absorber. In addition to deep La , N V , and C IV absorption, we have found intrinsic Si IV absorption at the same approximate radial velocity. The FOS observations are also described in Goodrich et al. (1998).

A.2. I Zw 1

Weak intrinsic absorption was discovered in the FOS spectra of this narrow-line Seyfert 1 galaxy by Laor et al. (1997). Although there are several observations, there is only one G130H spectrum, which contains the high-ionization absorption lines, and therefore no information is available on absorption variability.

A.3. NGC 3516

Intrinsic absorption lines of C IV , N V , and Si IV were originally detected in *IUE* spectra by Ulrich & Boisson (1983). NGC 3516 also exhibits a strong and variable X-ray warm absorber (Kolman et al. 1993; Nandra & Pounds 1994; Kriss et al. 1996b; Mathur, Wilkes, & Aldcroft 1997; George et al. 1998b). Intrinsic $\text{O VI} \lambda\lambda 1031.9, 1037.6$ absorption has been detected with the Hopkins Ultraviolet Telescope (*HUT*) by Kriss et al. (1996a). Kriss et al. have also detected intrinsic neutral hydrogen absorption (in the Lyman series) at a blueshift of -400 km s^{-1} , relative to the systemic velocity.

IUE monitoring found evidence for variability in the C IV absorption on time scales as small as weeks (Voit, Shull, & Begelman 1987, Walter et al. 1990; Kolman, Halpern, & Martin 1993). Walter et al. characterized the C IV absorption as a blend of a narrow stable component in the core of the emission-line, and a variable and broad blueshifted component. Kolman et al. (1993) found that $n_e \geq 10^5 \text{ cm}^{-3}$ and $r \leq 9 \text{ pc}$ for this variable component. Koratkar et al. (1996) show that the variable component disappeared between 1989 October and 1993 February, when there were no *IUE* observations, and has not reappeared.

Additional information on the FOS observations can be found in Goad et al. (1998), and a more detailed description of the GHRS observations is presented in Crenshaw et al. (1998). The variable blueshifted component of C IV has not reappeared in the *HST* spectra, and there is no evidence for variations in the remaining C IV absorption over the span of *HST* observations (1995 April - 1996 August).

A.4. NGC 3783

Intrinsic L α and C IV absorption were discovered in the FOS spectrum by Reichert et al. (1994), and intrinsic N V absorption was found by Lu, Savage, & Sembach (1994) in the GHRS spectra of this region. George et al. (1998a) found evidence for variability in the X-ray “warm absorber” between *ASCA* observations on 1993 December and 1996 July.

We presented the first two GHRS spectra of the C IV region in Maran et al. (1996), and discovered that the C IV absorption is extremely variable. We present the third GHRS spectrum of C IV in the current paper, and find that another C IV component has appeared at a higher blueshift (section 5). The C IV absorption detected in the GHRS spectrum on 1994 January 16 at -560 km s^{-1} could be the same component as that seen in the FOS spectrum on 1992 July 27 (at -660 km s^{-1}), given the weakness of the feature and the

wavelength uncertainties in the FOS spectra. This component completely disappeared on 1993 February 5, but is present in N V just 16 days later, on 1993 February 21, suggesting: 1) rapid variability, or 2) unusually high ionization during this time period (because in every Seyfert with simultaneous observations, C IV and N V absorption are always present together). As we discussed earlier, Shields & Hamann (1997) find $n_e \geq 300 \text{ cm}^{-3}$ and $r \leq 10 \text{ pc}$ for this component.

A.5. NGC 4151

A history of the early observations of intrinsic UV absorption is given in the Introduction. Previous observations of the complex X-ray absorption are described by George et al. (1998b). Observations with *HUT* and *ORFEUS* have extended the UV coverage down to 912 Å, and have resulted in the detection of a number of new absorption lines, including the strong lines of C III $\lambda 977.0$, N III $\lambda 989.8$, O VI $\lambda\lambda 1031.9, 1037.6$, and the hydrogen Lyman series (Kriss et al. 1992, 1995; Espey et al. 1998). Espey et al. show that the C III* $\lambda 1175$ (metastable) absorption line varies on a time scale of ~ 1 day, and thus $r \leq 25 \text{ pc}$, similar to the value obtained from H I absorption variations (Krolik & Kriss 1997). No variations were found in the high-ionization absorption lines (C IV, N V, O VI).

The FOS and GHRS spectra were obtained primarily by Weymann et al. (1997). Due to the large columns, widths, and number of components, the deconvolution of the C IV absorption is much more difficult than for any other object in this sample, even at high resolution. Weymann et al. present their deconvolution and measurement of individual components, and Kriss (1998) presents a slightly different deconvolution; we do not attempt to repeat their analyses here. Weymann et al. find no evidence for variations in the C IV absorption in five separate observations obtained over ~ 4 years, except for the appearance of a broad absorption feature in the blue wing of C IV on one occasion. They also present

evidence for variations in the S IV absorption in the low resolution spectra.

The only other line observed at high resolution is Mg II (Weymann et al. 1997). The Mg II/C IV ratio varies greatly from one component to the next, indicating a wide range in ionization parameter (Kriss 1998). NGC 4151 is the only object that shows Mg II absorption in our sample, and it would be interesting to test the uniqueness of this object, by looking for low-ionization absorption in other Seyfert 1 galaxies.

A.6. NGC 5548

The intrinsic C IV absorption was first studied in detail by Shull & Sachs (1993), using data from the 1988 - 1989 *IUE* monitoring campaign (Clavel et al. 1991). Shull & Sachs claim that C IV EW varies on a time scale of 4 days or less, and is anticorrelated with the continuum flux at 1570 Å, indicating that $n_e \geq 5 \times 10^5 \text{ cm}^{-3}$ and $r \leq 14 \text{ pc}$. Properties of the X-ray warm absorber are given by George et al. (1998b, and references therein).

The FOS observations that we used are from the 1993 *HST* monitoring campaign (Korista et al. 1995). Measurements of the absorption in these data are given by Mathur et al. (1995). We found no evidence for strong variations in these lines (given the difficulties imposed by low resolution), and therefore used the average spectrum from this campaign. The GHRS spectra of C IV (at low and high resolution) were obtained by Mathur et al. (1998), and the GHRS spectra of the N V region are also shown in Savage et al. (1997).

A.7. Mrk 509

York et al. (1984) found two kinematic components of intrinsic L α and C IV absorption in high-dispersion *IUE* spectra. Evidence for an X-ray warm absorber is given by Reynolds

(1997) and George et al. (1998b).

Our FOS observations found the same two kinematic components as those identified by York et al. (1984) ~ 12 years earlier, and we found N V at these velocities as well (Crenshaw et al. 1995). We originally agreed with the suggestion of York et al. (1984) that these components arise from extended regions of ionized gas in the host galaxy. However the high resolution GHRS spectra of $\text{L}\alpha$ (also shown in Savage et al. 1997) demonstrates that these two components are broad, and are likely to arise close to the nucleus. A determination of the location of the absorbers will require variability monitoring.

A.8. II Zw 136

We find intrinsic $\text{L}\alpha$, N V, and C IV absorption at two widely separated radial velocities in the GHRS low resolution spectra.

A.9. Akn 564

The absorption in this narrow-line Seyfert 1 galaxy is similar to that in WPVS 007, in that Si IV absorption is present in addition to strong $\text{L}\alpha$, N V, and C IV. The FOS observations are also presented by Goodrich et al. (1998).

A.10. NGC 7469

The FOS observations are also shown in Kriss et al. (1998). We find intrinsic $\text{L}\alpha$, N V, and C IV absorption at a large blueshift: -1770 km s^{-1} relative to the emission lines. George et al. (1998b) found marginal evidence for a warm absorber in *ASCA* spectra, whereas Reynolds (1997) found no absorption that satisfied his criteria.

B. Additional Seyfert 1 galaxies with possible intrinsic absorption

Although these Seyferts did not satisfy our selection criteria, they show broad La absorption, indicating possible intrinsic absorption close to the nucleus.

B.1. III Zw 2

A noisy FOS G130H spectrum obtained on 1992 January 18 shows moderately broad La absorption in the core of the emission profile, and possible intrinsic N V absorption, near the emission-line redshift of $z = 0.0894$.

B.2. Mrk 279

A high resolution GHRS spectra obtained on 1997 January 16 shows two broad, deep La absorption components, centered at -490 km s^{-1} and $+60 \text{ km s}^{-1}$ with respect to the emission-line redshift ($z = 0.0306$).

B.3. Mrk 290

A high resolution GHRS spectra obtained on 1997 January 9 shows a broad, deep La absorption component, centered at -240 km s^{-1} relative to the emission-line redshift ($z = 0.0296$).

REFERENCES

Anderson, K.S. 1974, *ApJ*, 189, 195

Anderson, K.S., & Kraft, R.P. 1969, *ApJ*, 158, 859

Blackwell, J., Shore, S.N., Robinson, R.D., Feggans, K. Lindler, D., Malumuth, E., Sandoval, J., and Ake, T.B. 1993, A User's Guide to the GHRS Software, Version 2.1

Boksenberg, A., et al. 1978, *Nature*, 275, 404

Bromage, G.E., et al. 1985, *MNRAS*, 215, 1

Clavel, J., et al. 1991, *ApJ*, 366, 64

Crenshaw, D.M. 1997, in Emission Lines in Active Galaxies: New Methods and Techniques, ed. B.M. Peterson, F.-Z. Cheng, and A.S. Wilson (San Francisco: Astronomical Society of the Pacific), *ASP Conference Series*, 113, 240

Crenshaw, D.M., Boggess, A., and Wu, C.-C. 1995, *AJ*, 110, 1026

Crenshaw, D.M., Maran, S.P., & Mushotzky, R.F. 1998, *ApJ*, 496, 797

Crenshaw, D.M., & Peterson, B.M. 1985, *ApJ*, 291, 677

Cromwell, R., & Weymann, R. 1970, *ApJ*, 159, L147

Davidsen, A.F., & Hartig, G.F. 1978, in Proc. COSPAR/IAU Symp. on X-ray Astronomy, ed. W.A. Baity & L.E. Peterson (Oxford: Pergamon Press), p. 377

Espey, B.R., Kriss, G.A., Krolik, J.H., Zheng, W., Tsvetanov, Z., & Davidsen, A.F. 1998, *ApJ*, 500, L13

Ferland, G.J., & Mushotzky, R.F. 1982, *ApJ*, 262, 564

Ferland, G.J., et. al. 1992, *ApJ*, 387, 95

Gaskell, C.M. 1982, *ApJ*, 263, 79

George, I.M., Turner, T.J., Mushotzky, R., Nandra, K. & Netzer, H. 1998a, *ApJ*, in press

George, I.M., Turner, T.J., Netzer, H., Nandra, K., Mushotzky, R.F., and Yaqoob, T. 1998b, ApJS, 114, 73

Goad, M.R., et al. 1998, in preparation

Goodrich, R.W. 1998, in preparation

Grupe, D., Beuerman, K., Mannheim, K., Thomas, H.-C., Fink, H.H., & de Martino, D. 1995, A&A, 300, L21

Halpern, J.P. 1984, ApJ, 281, 90

Hamann, F. 1997, ApJS, 109, 279

Hamann, F., Barlow, T.A., Junkkarinen, V. & Burbidge, E.M. 1997, ApJ, 478, 87

Keyes, C.D., et al. 1995, Faint Object Spectrograph Instrument Handbook, Version 6.0

Khachikian, E.Ye., & Weedman, D.W. 1971, Astrofizika, 7, 389

Kolman, M. Halpern, J.P., Martin, C., Awaki, H., & Koyama, K. 1993, ApJ, 403, 592

Koratkar, A., et al. 1996, ApJ, 470, 378

Korista, K.T., et al. 1995, ApJS, 97, 285

Koski, A.T. 1978, ApJ, 223, 56

Krolik, J.H., & Kriss, G.A. 1997, in Mass Ejection from Active Galactic Nuclei, ed. N. Arav, I. Shlosman, & R.J. Weymann, (San Francisco: Astronomical Society of the Pacific), ASP Conference Series, 128, 132

Kriss, G.A. 1998, in The Scientific Impact of the Goddard High Resolution Spectrograph, ed. J.C. Brandt, T.B. Ake III, and C.C. Peterson, (San Francisco: Astronomical Society of the Pacific) ASP Conference Series, 143, 271

Kriss, G.A., et al. 1992, ApJ, 392, 485

Kriss, G.A., Davidsen, A.F., Zheng, W., Kruk, J.W., & Espey, B.R. 1995, ApJ, 454, L7

Kriss, G.A., Espey, B.R., Krolik, J.H., Tsvetanov, Z., Zheng, W., & Davidsen, A.F. 1996a, ApJ, 467, 622

Kriss, G.A., et al. 1996b, ApJ, 467, 629

Kriss, G., Krolik, J., Grimes, J., Tsvetanov, Z., Zheng, W., & Davidsen, A. 1996c, in proc. IAU Colloquium 159, Emission Lines in Active Galaxies: New Methods and Techniques, eds. B.M. Peterson, F.-Z. Cheng, & A.S. Wilson (Astronomical Society of the Pacific: San Francisco), 113, 453.

Kriss, G.A., et al. 1998, in preparation

Laor, A., Jannuzzi, B.T., Green, R.F., & Boroson, T.A. 1997, ApJ, 489, 656

Lu, L., Savage, B.D., & Sembach, K.R. 1994, ApJ, 426, 563

Maran, S.P., et al. 1996, ApJ, 465, 733

Mathur, S. 1994, ApJ, 431, L75

Mathur, S., et al. 1998, in preparation

Mathur, S., Elvis, M., & Wilkes, B. 1995, ApJ, 452, 230

Mathur, S., Wilkes, B., & Aldcroft, T. 1997, ApJ, 478, 182

Mathur, S., Wilkes, B., Elvis, M., & Fiore, F. 1994, ApJ, 434, 493

Morton, D.C., York, D.G., & Jenkins, E.B. 1988, ApJS, 68, 449

Nandra, P., & Pounds, K.A. 1994, MNRAS, 268, 405

Oke, J.B., & Sargent, W.L.W. 1968, ApJ, 151, 807

Osterbrock, D.E. 1981, ApJ, 249, 462

Osterbrock, D.E. 1984, QJRAS, 25, 1

Osterbrock, D.E., & Pogge, R.W. 1985, ApJ, 297, 166

Penston, M.V., et al. 1981, MNRAS, 196, 857

Reichert, G.A., et al. 1994, *ApJ*, 425, 582

Reynolds, C.S. 1997, *MNRAS*, 286, 513

Reynolds, C.S., & Fabian, A.C. 1995, *MNRAS*, 273, 1167

Savage, B.D., & Sembach, K.R. 1991, *ApJ*, 379, 245

Savage, B.D., Sembach, K.R., & Lu, L. 1997, *AJ*, 113, 2158

Seyfert, C.K. 1943, *ApJ*, 97, 28

Shields, J.C., & Hamann, F. 1997, *ApJ*, 481, 752

Shull, J.M., & Sachs, E.R. 1993, *ApJ*, 416, 536

Shull, J.M., Stocke, J.T., and Penton, S. 1996, *AJ*, 111, 72

Soderblom, D.R., et al. 1995, Instrument Handbook for the Goddard High Resolution Spectrograph, Version 6.0

Spitzer, L. 1978, Physical Processes in the Interstellar Medium (New York: John Wiley), 51

Stocke, J.T., et al. 1995, *ApJ*, 451, 24

Ulrich, M.-H. 1988, *MNRAS*, 230, 121

Ulrich, M.-H. & Boisson, C. 1983, *ApJ*, 267, 515

Voit, G.M., Shull, J.M., & Begelman, C. 1987, *ApJ*, 316, 573

Vrtilek, J.M., & Carleton, N.P. 1985, *ApJ*, 294, 106

Walter, R., Ulrich, M.-H., Courvoisier, T.J.-L., & Buson, L.M. 1990, *A&A*, 233, 53

Wanders, I. et al., 1997, *ApJS*, 113, 69

Weedman, D.W. 1977, *ARA&A*, 15, 69

Weymann, R.J., Carswell, R.F., & Smith, M.G. 1981, *ARA&A*, 19, 41

Weymann, R.J., Foltz, C.B., & Hewett, P.C. 1991, *ApJ*, 373, 23

Weymann. R.J., Morris, S.L., Gray, M.E., & Hutchings, J.B. 1997, ApJ, 483, 717

Wu, C.-C., Boggess, A., and Gull, T.R. 1983, ApJ, 266, 28

York, D.G., Ratcliff, S., Blades, J.C., Cowie, L.L., Morton, D.C., & Wu, C.-C. 1984, ApJ, 276, 92

Fig. 1.— Far-UV low resolution spectra of seven Seyfert 1 galaxies that do not show intrinsic UV absorption. The positions of the strong Galactic lines are noted at the bottom.

Fig. 2.— Far-UV low resolution spectra of 10 Seyfert 1 galaxies that show intrinsic UV absorption. The positions of the intrinsic absorption lines are labeled, and the positions of the strong Galactic lines are noted at the bottom.

Fig. 3.— GHRS high resolution spectra of the C IV region in four Seyfert 1 galaxies. The kinematic components are numbered, beginning at the shortest wavelengths, and Galactic lines are labeled with a “G”.

Fig. 4.— GHRS high resolution spectra of other lines in this sample. The kinematic components are numbered, beginning at the shortest wavelengths, and Galactic lines are labeled with a “G”. For the high resolution spectrum of Mg II in NGC 4151, see Weymann et al. (1997).

Table 1. Observations

Name	Inst.	Gratings	Coverage ^a	Aper. ^b ('")	Observation Date (UT)
Low resolution spectra					
Mrk 335	FOS	G130H, G190H, G270H	1150 - 3280	1.0	1994 December 16
WPVS 007	FOS	G130H, G190H, G270H	1150 - 3280	1.0	1996 July 30
I Zw 1 (1)	FOS	G270H	2220 - 3280	1.0	1992 July 29
I Zw 1 (2)	FOS	G190, G270H	1575 - 3280	4.3	1993 January 16
I Zw 1 (3)	FOS	G130H	1150 - 1605	1.0	1994 February 13
I Zw 1 (4)	FOS	G190H, G270H	1575 - 3280	1.0	1994 September 14
Fairall 9	FOS	G130H, G190H, G270H	1150 - 3280	1.0	1993 January 22
NGC 1566	FOS	G130H, G190H, G270H	1150 - 3280	1.0	1994 February 8, 11
Akn 120	FOS	G130H, G190H, G270H	1150 - 3280	1.0	1995 1995 July 29
NGC 3516 (1)	FOS	G130H, G190H, G270H	1150 - 3280	1.0	1995 December 30
NGC 3516 (2)	FOS	G130H, G190H, G270H	1150 - 3280	1.0	1996 February 21
NGC 3516 (3)	FOS	G130H, G190H, G270H	1150 - 3280	1.0	1996 April 13
NGC 3516 (4)	FOS	G130H, G190H G270H	1150 - 3280	1.0	1996 November 28
NGC 3516 (5)	FOS	G130H, G190H, G270H	1150 - 3280	1.0	1996 August 14
NGC 3783	FOS	G130H, G190H	1150 - 2330	1.0	1992 July 27
NGC 4151 (1)	FOS	G130H	1150 - 1605	1.0	1992 June 22 - 27
NGC 4151 (2)	FOS	G130H	1150 - 1605	0.25x2.0	1992 July 3
NGC 4151 (3)	FOS	G270H	2220 - 3280	0.3	1993 April 22
NGC 4151 (4)	FOS	G130H	1150 - 1605	0.3	1996 March 11
Mrk 205 (1)	FOS	G190H, G270H	1575 - 3280	0.25x2.0	1991 July 11
Mrk 205 (2)	FOS	G130H	1150 - 1605	4.3	1993 July 18
NGC 5548 (1)	FOS	G130H, G190H, G270H	1150 - 3280	1.0	1992 July 5
NGC 5548 (2)	FOS	G130H, G190H	1150 - 2330	4.3	1993 April 19 - May 27
NGC 5548 (3)	GHRS	G140L	1415 - 1715	2.0	1996 August 24
Mrk 478	FOS	G130H, G190H, G270H	1150 - 3280	1.0	1996 December 5
Mrk 493	FOS	G130H, G190H, G270H	1150 - 3300	1.0	1996 September 4
Mrk 509	FOS	G130H, G190H, G270H	1150 - 3300	1.0	1992 June 21

Table 1—Continued

Name	Inst.	Gratings	Coverage ^a	Aper. ^b (")	Observation Date (UT)
II Zw 136	GHRS	G140L	1153 - 1740	2.0	1995 July 24
Akn 564	FOS	G130H, G190H, G270H	1150 - 3280	1.0	1996 May 23
NGC 7469	FOS	G130H, G190H, G270H	1150 - 3300	1.0	1996 June 18
High resolution spectra					
NGC 3516 (1)	GHRS	G160M	C IV	2.0	1995 April 25
NGC 3516 (2)	GHRS	G160M	C IV	2.0	1995 October 22
NGC 3783 (1)	GHRS	G160M	N V	2.0	1993 February 21
NGC 3783 (2)	GHRS	G160M	C IV	2.0	1993 February 5
NGC 3783 (3)	GHRS	G160M	C IV	2.0	1994 January 16
NGC 3783 (4)	GHRS	G160M	C IV	2.0	1995 April 11
NGC 4151 (1)	GHRS	G160M	C IV	2.0	1992 July 4
NGC 4151 (2)	GHRS	G160M, G270M	C IV, Mg II	2.0	1994 January 3
NGC 4151 (3)	GHRS	G160M, G270M	C IV, Mg II	2.0	1994 October 28 - 29
NGC 4151 (4)	GHRS	G160M, G270M	C IV, Mg II	2.0	1996 March 11
NGC 5548 (1)	GHRS	G160M	L α , N V	2.0	1996 February 17
NGC 5548 (2)	GHRS	G160M	C IV	2.0	1996 August 24
Mrk 509	GHRS	G160M	L α	2.0	1993 May 22

^aFor the low resolution spectra, coverage is given in Å. For the high resolution spectra, coverage is specified by the emission-line profile that is present.

^bThe shapes and exact dimensions of the apertures, before and after the installation of COSTAR in 1993 December, are given in Keyes et al. 1995 and Soderblom et al. 1995.

Table 2. Redshifts and intrinsic absorption detections

Name	z (H I)	z (optical) ^a	Intrinsic UV Absorption?	X-ray Warm Absorber?
Mrk 335		0.02564	No	No
WPVS 007 ^b		0.02882	Yes	
I Zw 1 ^b	0.06108	0.06072	Yes	
Fairall 9		0.04614	No	No
NGC 1566	0.00499	0.00483	No	
Akn 120		0.03312	No	
NGC 3516		0.00875	Yes	Yes
NGC 3783		0.00976	Yes	Yes
NGC 4151	0.00332	0.00319	Yes	Yes
Mrk 205		0.07085	No	
NGC 5548	0.01717	0.01676	Yes	Yes
Mrk 478		0.07905	No	
Mrk 493 ^b	0.03148	0.03131	No	
Mrk 509		0.03440	Yes	Yes
II Zw 136	0.06298	0.06305 ^c	Yes	
Akn 564 ^b	0.02467	0.02499	Yes	
NGC 7469	0.01640	0.01616	Yes	Yes? ^d

^aPrimarily from the narrow [O III] lines.^bNarrow-line Seyfert 1.^cfrom Vrtilek & Carleton (1985).^dYes according to George et al. (1998); no according to Reynolds (1997).

Table 3. Direct measurements of low resolution spectra

Name	λ_{obs} (Å)	EW (Å)	Line (Component)	v_r (km s ⁻¹)
WPVS 007	1249.13	1.69±0.19	L α	-390
	1273.08	1.80±0.34	N V λ 1238.8	-348
	1277.22	1.76±0.29	N V λ 1242.8	-336
	1432.20	1.06±0.32	Si IV λ 1393.8	-369
	1440.48	0.72±0.33	Si IV λ 1402.8	-366
	1590.76	2.59±0.41	C IV λ 1548.2	-399
	1593.85	2.29±0.23	C IV λ 1550.8	-311
I Zw 1	1280.88	0.49±0.07	L α	-2122
	1305.08	0.68±0.07	N V λ 1238.8	-2167
	1309.90	0.27±0.05	N V λ 1242.8	-2017
	1631.07	0.63±0.11	C IV λ 1548.2	-2155
	1633.95	0.26±0.10	C IV λ 1550.8	-2123
NGC 3516 ^a	1225.60	1.87±0.07	L α	-174
	1249.29	1.62±0.03	N V λ 1238.8	-90
	1253.20	1.54±0.06	N V λ 1242.8	-114
	1404.82	0.47±0.06	Si IV λ 1393.8	-243
	1413.82	0.31±0.06	Si IV λ 1402.8	-261
	1561.08	1.73±0.11	C IV λ 1548.2	-128
	1563.69	1.55±0.10	C IV λ 1550.8	-126
NGC 3783	1224.79	0.81±0.07	L α	-677
	1248.07	0.18±0.03	N V λ 1238.8	-686
	1253.1	—	N V λ 1242.8, Gal. S II λ 1253.8	—
	1560.17	0.12±0.04	C IV λ 1548.2	-608
	1562.93	0.07±0.03	C IV λ 1550.8	-575

Table 3—Continued

Name	λ_{obs} (Å)	EW (Å)	Line (Component)	v_r (km s ⁻¹)
NGC 4151 ^a	1214.76	—	L α , Gal. L α	—
	1240.63	3.04±0.32	N V λ 1238.8	-519
	1244.86	2.49±0.22	N V λ 1242.8	-459
	1396.32	1.92±0.32	Si IV λ 1393.8	-405
	1405.73	1.19±0.19	Si IV λ 1402.8	-323
	1549.58	3.76±0.51	C IV λ 1548.2	-689
	1553.73	2.84±0.39	C IV λ 1550.8	-384
NGC 5548 ^a	1234.45	0.73±0.06	L α	-393
	1258.71	—	N V λ 1238.8, Gal. Si II λ 1260.4	—
	1261.66	—	N V λ 1242.8, Gal. Si II λ 1260.4	—
	1572.60	C IV λ 1548.2	0.23±0.04	-300
	1575.74	C IV λ 1550.8	0.12±0.02	-200
Mrk 509	1255.80	0.48±0.11	L α (1)	-417
	1257.64	1.54±0.04	L α (2)	+36
	1279.77	0.25±0.05	N V λ 1238.8 (1)	-399
	1281.27	0.50±0.06	N V λ 1238.8 (2)	-36
	1283.81	0.17±0.06	N V λ 1242.8 (1)	-420
	1285.39	0.28±0.05	N V λ 1242.8 (2)	-40
	— ^b	—	C IV λ 1548.2 (1), C IV λ 1550.8 (1), C IV λ 1548.2 (2), C IV λ 1550.8 (2)	—

Table 3—Continued

Name	λ_{obs} (Å)	EW (Å)	Line (Component)	v_r (km s ⁻¹)
II Zw 136	1286.07	0.38±0.04	L α (1)	-1541
	1292.53	0.17±0.02	L α (2)	+52
	1310.57	0.37±0.07	N V λ 1238.8 (1)	-1539
	1314.75	0.26±0.05	N V λ 1242.8 (1)	-1546
	1317.19	0.14±0.03	N V λ 1238.8 (2)	+63
	1321.58	0.09±0.03	N V λ 1242.8 (2)	+101
	1637.62	0.46±0.06	C IV λ 1548.2 (1)	-1587
	1640.12	0.29±0.05	C IV λ 1550.8 (1)	-1629
	1645.81	0.10±0.03	C IV λ 1548.2 (2)	-1
	1648.61	0.06±0.03	C IV λ 1550.8 (2)	+12
Akn 564	1245.40	1.85±0.13	L α	-159
	1269.13	1.89±0.24	N V λ 1238.8	-157
	1273.26	1.49±0.26	N V λ 1242.8	-144
	1427.54	0.56±0.18	Si IV λ 1393.8	-224
	1436.71	0.44±0.15	Si IV λ 1402.8	-240
	1586.14	1.69±0.14	C IV λ 1548.2	-144
	1588.89	1.63±0.17	C IV λ 1550.8	-123
NGC 7469	1227.97	0.38±0.07	L α	-1810
	1251.53	0.33±0.07	N V λ 1238.8	-1814
	1255.70	0.16±0.08	N V λ 1242.8	-1732
	1564.24	0.26±0.07	C IV λ 1548.2	-1738
	1566.80	0.16±0.06	C IV λ 1550.8	-1745

^aNo evidence for variability; average values are given.^bA deconvolution of the components in given in Crenshaw et al. (1995).

Table 4. Direct measurements of high resolution spectra^a

Name (Epoch)	λ_{obs} (Å)	EW (Å)	Line (Component)	v_r (km s ⁻¹)	FWHM (km s ⁻¹)
NGC 3516 (1)	1559.87	0.75±0.04	C IV λ 1548.2 (1)	-375	138
	1561.04	1.11±0.04	C IV λ 1548.2 (2)	-148	220
	1561.34	0.04±0.02	C IV λ 1548.2 (3)	-90	17
	1561.63	0.08±0.02	C IV λ 1548.2 (4)	-34	29
	1562.44	0.59±0.02	C IV λ 1550.8 (1)	-379	121
	1563.63	0.99±0.02	C IV λ 1550.8 (2)	-149	207
	1563.96	0.04±0.02	C IV λ 1550.8 (3)	-85	17
	1564.23	0.07±0.02	C IV λ 1550.8 (4)	-33	25
NGC 3516 (2)	1559.87	0.68±0.03	C IV λ 1548.2 (1)	-375	127
	1561.06	1.16±0.05	C IV λ 1548.2 (2)	-144	207
	1561.35	0.06±0.04	C IV λ 1548.2 (3)	-88	23
	1561.65	0.09±0.03	C IV λ 1548.2 (4)	-30	34
	1562.44	0.56±0.03	C IV λ 1550.8 (1)	-379	119
	1563.62	1.03±0.04	C IV λ 1550.8 (2)	-151	190
	1563.95	0.03±0.02	C IV λ 1550.8 (3)	-87	23
	1564.26	0.06±0.03	C IV λ 1550.8 (4)	-27	36
NGC 3783 (1)	1248.58	0.28±0.04	N V λ 1238.8 (2)	-563	180
	1252.57	0.19±0.03	N V λ 1242.8 (2)	-569	179
NGC 3783 (3) ^b	1560.46	—	C IV λ 1548.2 (2), Gal. C I λ 1560.3	—	—
	1563.01	0.14±0.01	C IV λ 1550.8 (2)	-561	134
NGC 3783 (4)	1556.07	0.39±0.08	C IV λ 1548.2 (1)	-1403	370
	1558.44	0.14±0.08	C IV λ 1550.8 (1)	-1442	320
	1560.44	—	C IV λ 1548.2 (2), Gal. C I λ 1560.3	—	—
	1563.01	0.13±0.03	C IV λ 1550.8 (2)	-560	152

Table 4—Continued

Name (Epoch)	λ_{obs} (Å)	EW (Å)	Line (Component)	v_r (km s ⁻¹)	FWHM (km s ⁻¹)	
NGC 5548 (1)	1255.32	0.34±0.05	N V λ 1238.8 (1)	−1031	114	
	1256.84	0.09±0.03	N V λ 1238.8 (2)	−1663	52	
	1257.40	0.41±0.06	N V λ 1238.8 (3)	−528	—	
	1258.18	0.59±0.04	N V λ 1238.8 (4)	−339	188	
	1258.90	0.22±0.04	N V λ 1238.8 (5), N V λ 1242.8 (1)	—	—	
	1260.95	0.09±0.03	N V λ 1242.8 (2)	−647	—	
	1261.54	0.36±0.03	N V λ 1242.8 (3)	−504	—	
	1262.25	0.47±0.04	N V λ 1242.8 (4)	−373	—	
	1262.91	0.09±0.02	N V λ 1242.8 (5)	−174	57	
	1568.53	0.05±0.02	C IV λ 1548.2 (1)	−1088	—	
NGC 5548 (2)	1570.72	0.09±0.01	C IV λ 1548.2 (2)	−662	38	
	1571.41	0.29±0.03	C IV λ 1548.2 (3), C IV λ 1550.8 (1)	—	—	
	1572.43	0.62±0.04	C IV λ 1548.2 (4)	−333	145	
	1573.27	0.09±0.02	C IV λ 1548.2 (5) C IV λ 1550.8 (2)	—	—	
	1574.07	0.10±0.03	C IV λ 1550.8 (3)	−521	90	
	1575.06	0.45±0.04	C IV λ 1550.8 (4)	−330	135	
	1575.95	0.07±0.03	C IV λ 1550.8 (5)	−156	90	
	Mrk 509	1256.15	0.83±0.03	L α (1)	−330	215
		1257.78	1.52±0.02	L α (2)	+72	367

^aMeasurements for NGC 4151 are given by Weymann et al. 1997.^bNo intrinsic absorption was detected in epoch 2 (Maran et al. 1996).

Table 5. Kinematic components in the low resolution spectra

Name	Component	v_r (km s $^{-1}$)
WPVS 007	1	–360±31
I Zw 1	1	–2117±59
NGC 3516	1	–162±66
NGC 3783	1	–657±43
NGC 4151	1	–463±129
NGC 5548	1	–298±96
Mrk 509	1	–412±11
	2	–13±42
II Zw 136	1	–1568±39
	2	+45±41
Akn 564	1	–170±44
NGC 7469	1	–1768±40

Table 6. Kinematic components and covering factors in the high resolution spectra

Name	Component	v_r (km s $^{-1}$)	FHWM (km s $^{-1}$)	C_{los}	C_{los}^{BLR}	Line a
NGC 3516	1	−377±2	126±9	0.99±0.01	0.99	(C IV)
	2	−148±3	206±12	0.98±0.01	0.97	(C IV)
	3	−88±2	20±4	≥0.83	≥0.79	(C IV)
	4	−31±3	31±5	≥0.74	≥0.67	(C IV)
NGC 3783	1	−1422±28	345±35	≥0.21	≥−0.45	(C IV)
	2	−563±4	161±22	0.52±0.25	0.14	(N V)
NGC 4151 b	—	—	—	≥0.94	≥0.93	(C IV)
NGC 5548	1	−1060±40	114±10	≥0.52	≥0.23	(N V)
	2	−655±11	45±10	≥0.76	≥0.72	(L α)
	3	−518±12	90±10	≥0.81	≥0.79	(L α)
	4	−344±20	156±28	0.96±0.04	0.95	(C IV)
	5	−165±13	74±23	≥0.69	≥0.66	(L α)
Mrk 509	1	−330±10	215±10	≥0.91	≥0.90	(L α)
	2	+72±10	367±10	≥0.93	≥0.92	(L α)

 a Line from which the covering factors were determined. b From component “E” in Weymann et al. (1997) – see this reference for additional measurements.

Table 7. Column densities for high resolution spectra

Name (Epoch)	Ion	Comp.	N (10^{14} cm $^{-2}$) ^a	
NGC 3516 (1)	C IV	1	8.0±0.5	(8.4±0.5)
	C IV	2	13.7±1.2	(15.3±1.3)
	C IV	3	0.4±0.1	
	C IV	4	0.5±0.1	
NGC 3516 (2)	C IV	1	6.3±0.5	(6.6±0.5)
	C IV	2	11.0±2.4	(15.4±3.3)
	C IV	3	0.4±0.1	
	C IV	4	0.5±0.1	
NGC 3783 (1)	N V	1	<0.04	
	N V	2	2.4±0.5	(5.2±1.1)
NGC 3783 (2)	C IV	1	<0.05	
	C IV	2	<0.03	
NGC 3783 (3)	C IV	1	<0.05	
	C IV	2	0.9±0.1	
NGC 3783 (4)	C IV	1	1.2±0.2	
	C IV	2	0.9±0.3	
NGC 5548 (1)	N V	1	2.0±0.3	
	N V	2	0.6±0.2	
	N V	3	3.9±0.3	
	N V	4	6.5±0.5	(8.4±0.7)
	N V	5	1.1±0.2	
	C IV	1	0.11±0.04	
NGC 5548 (2)	C IV	2	0.28±0.04	
	C IV	3	0.48±0.15	
	C IV	4	2.89±0.22	(3.13±0.24)
	C IV	5	0.41±0.18	

^aThe first value assumes $C_{los} = 1$. The value in parentheses was calculated using the C_{los} value in Table 6.

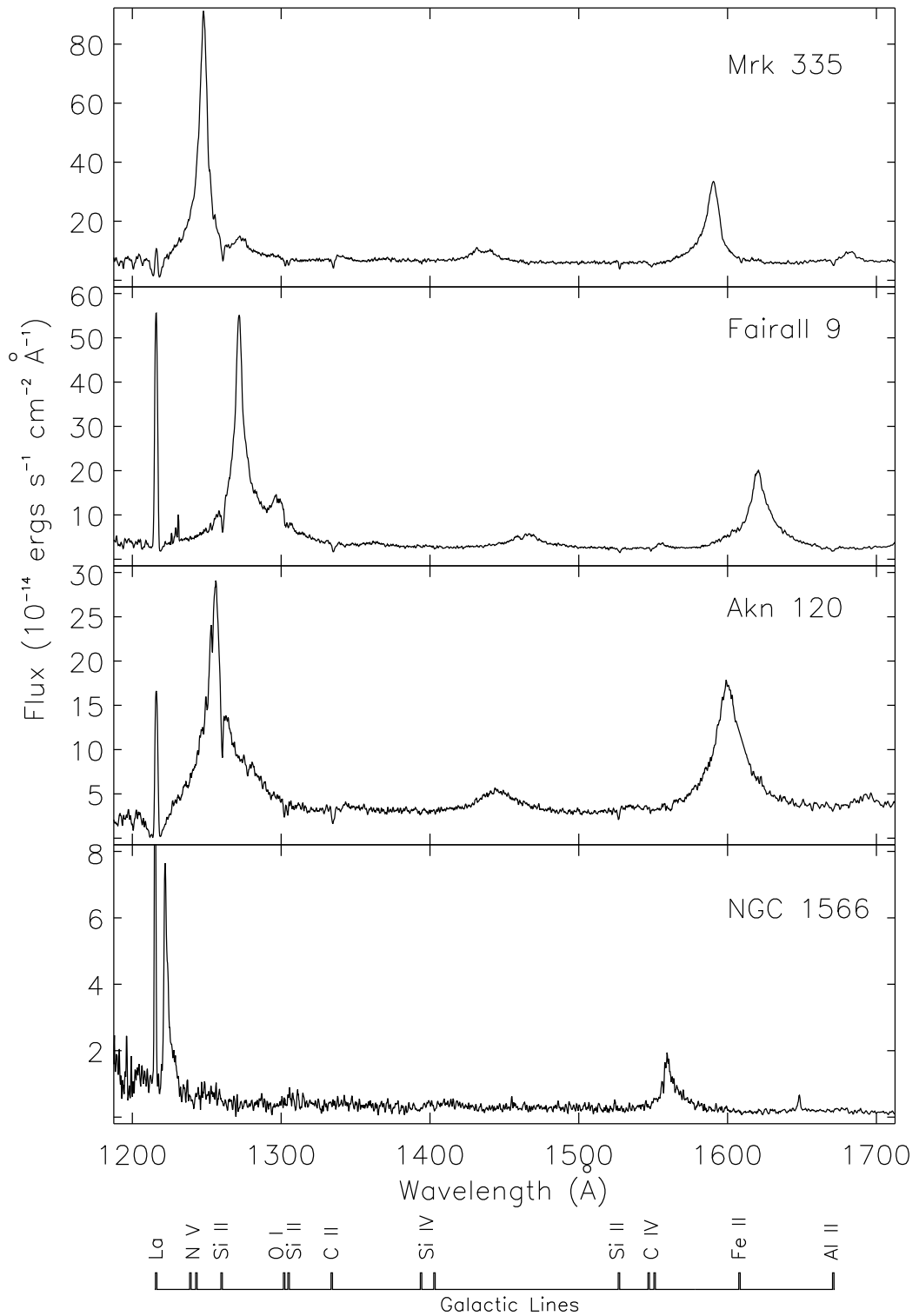


Fig. 1.

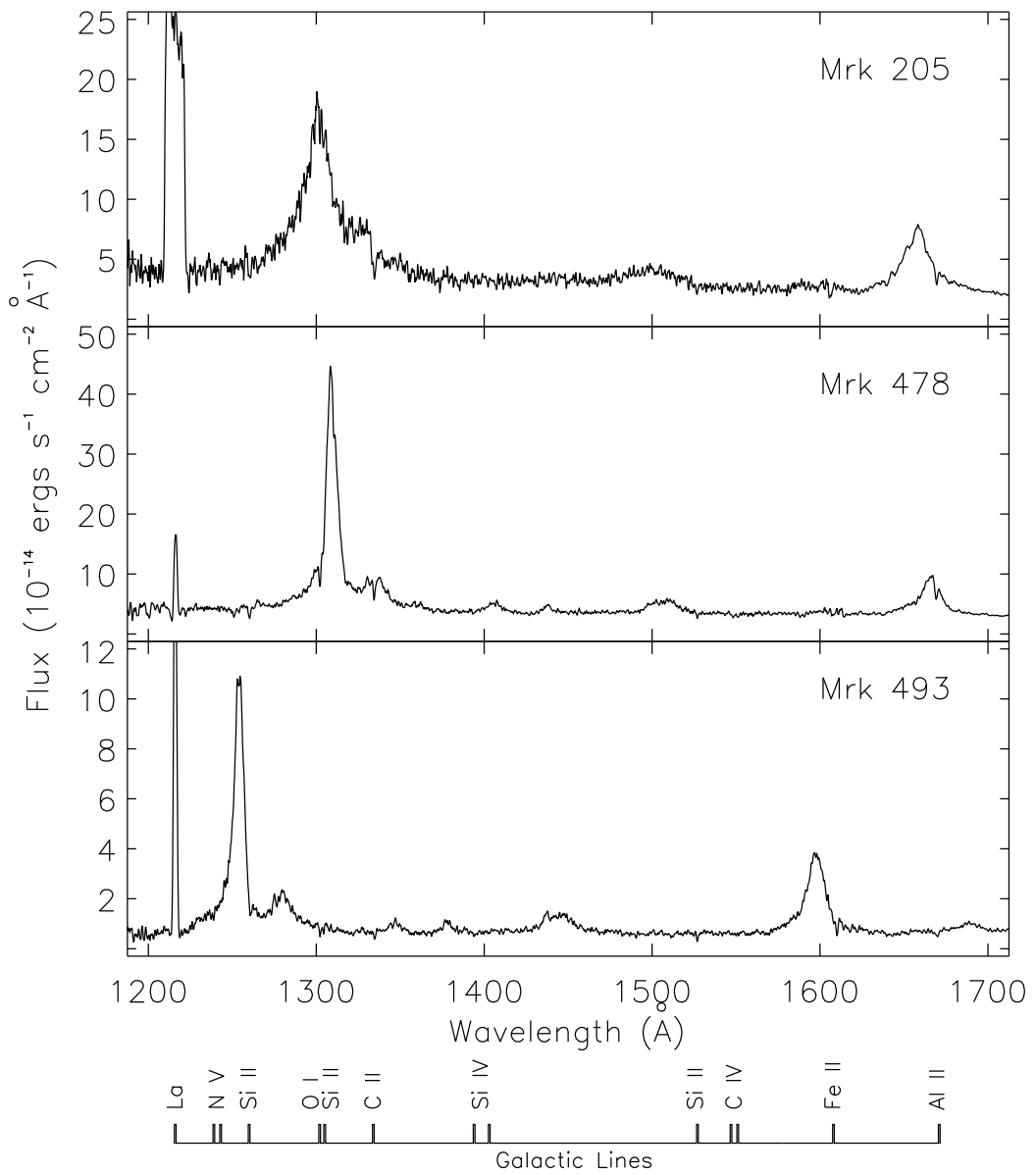


Fig. 1.–Continued

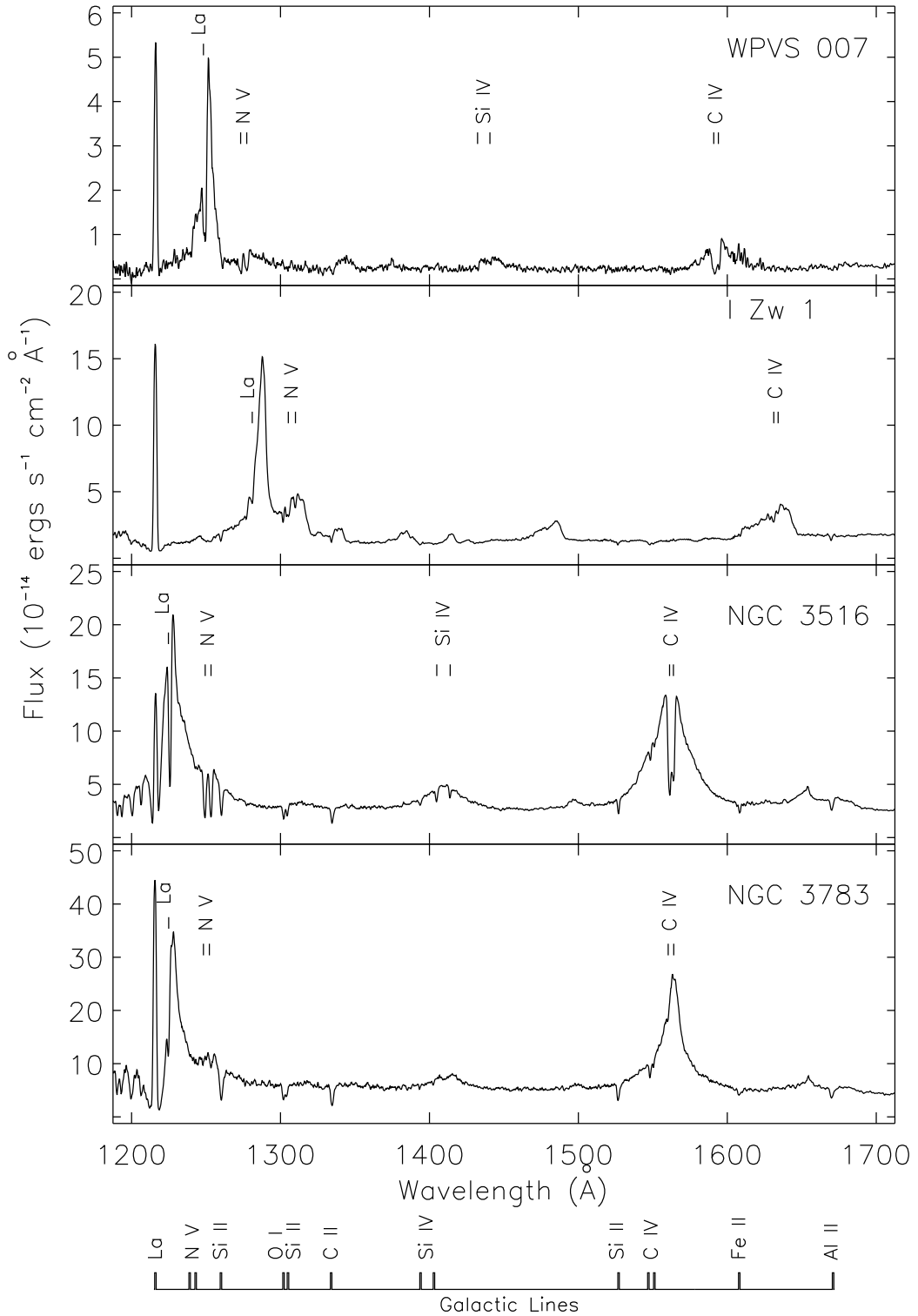


Fig. 2.

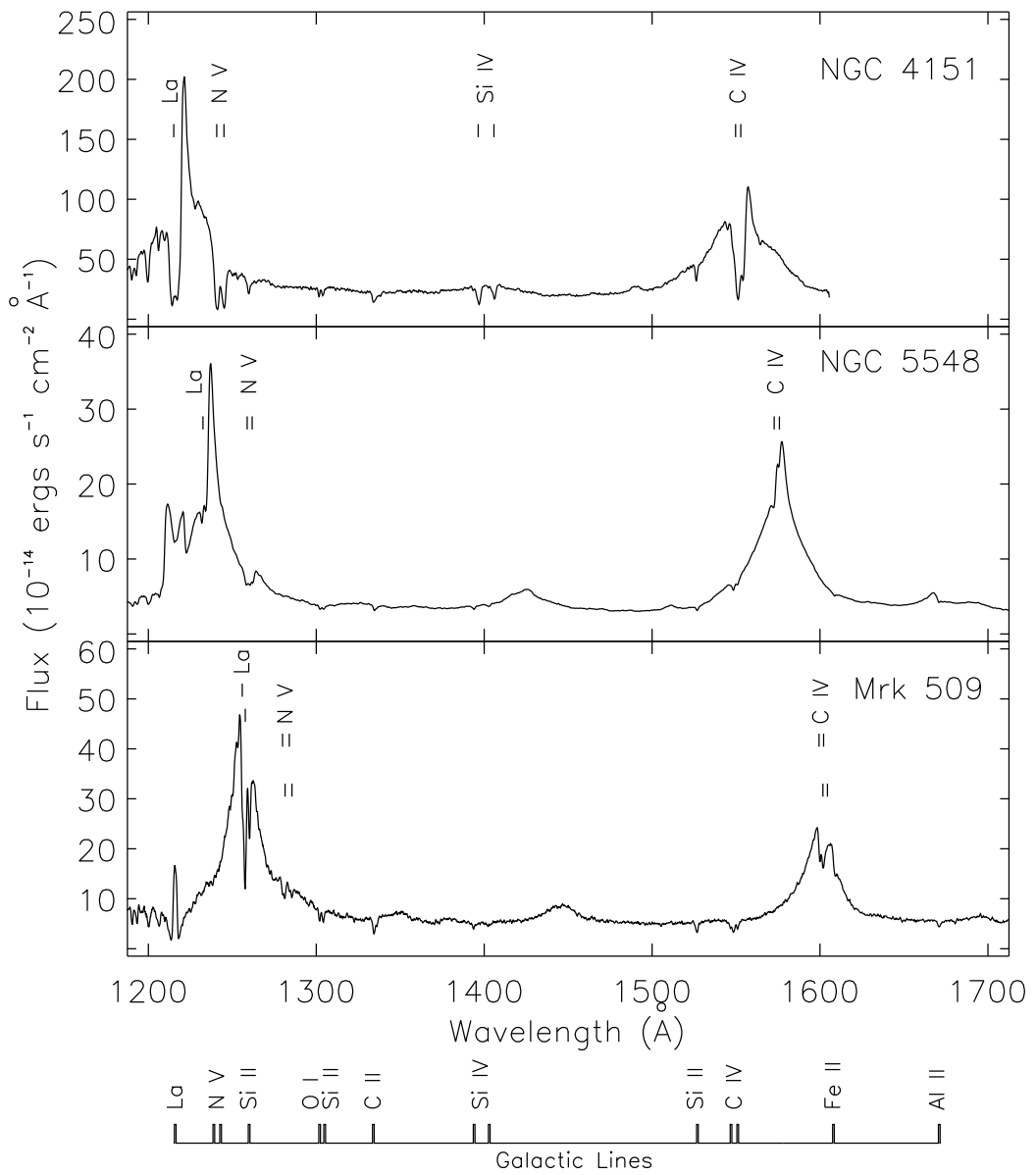


Fig. 2.—Continued

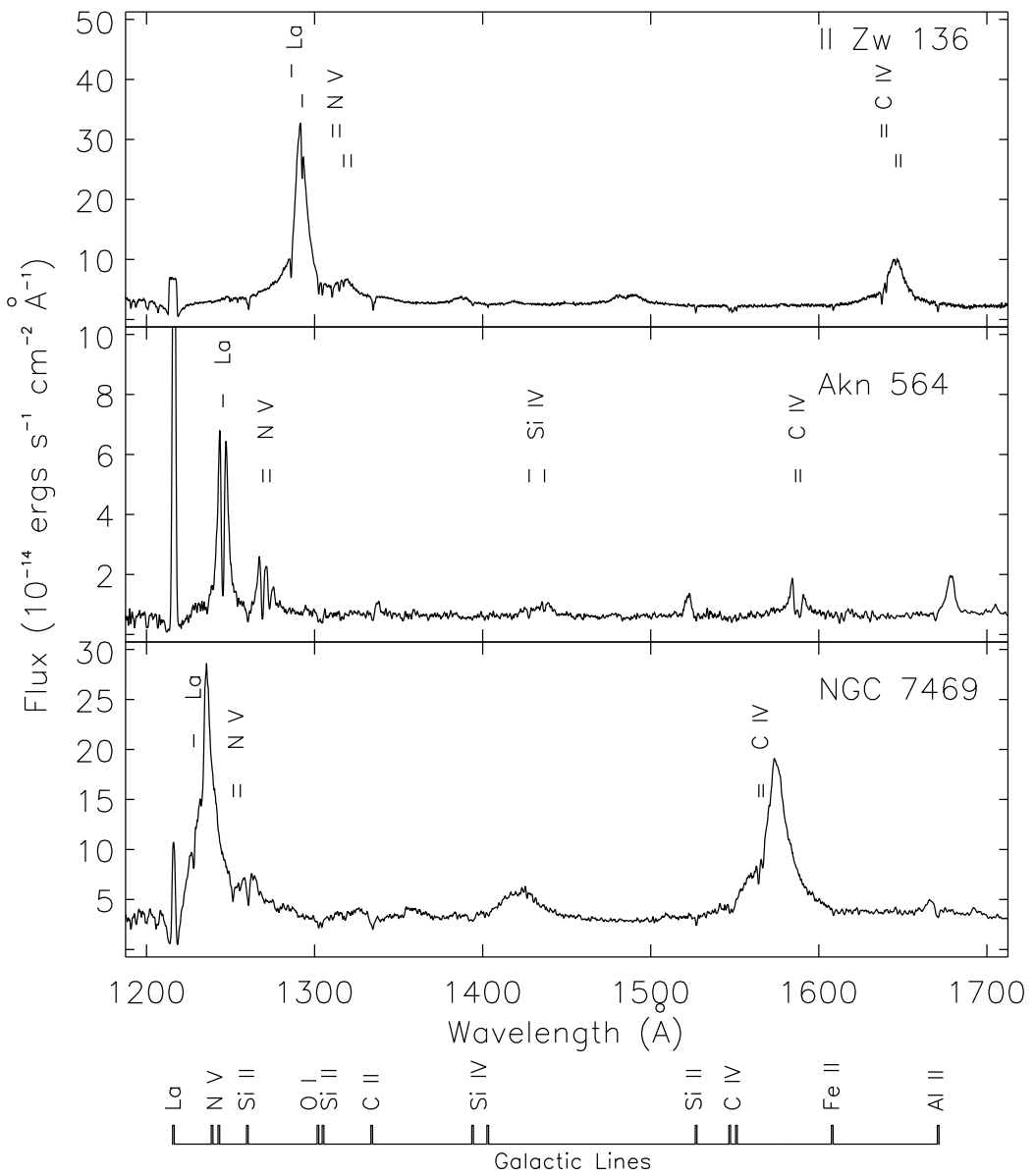


Fig. 2.—Continued

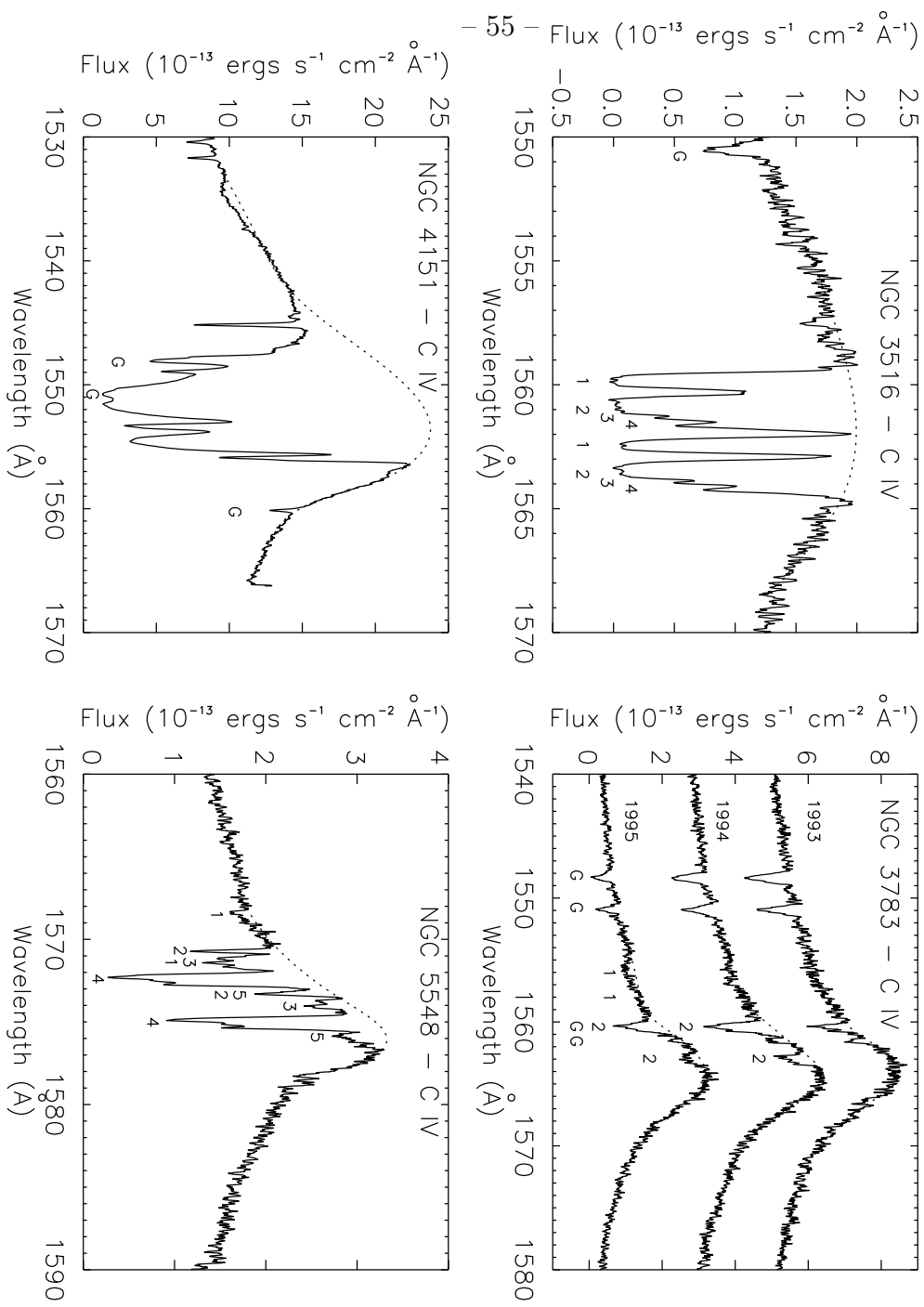


Fig. 3.

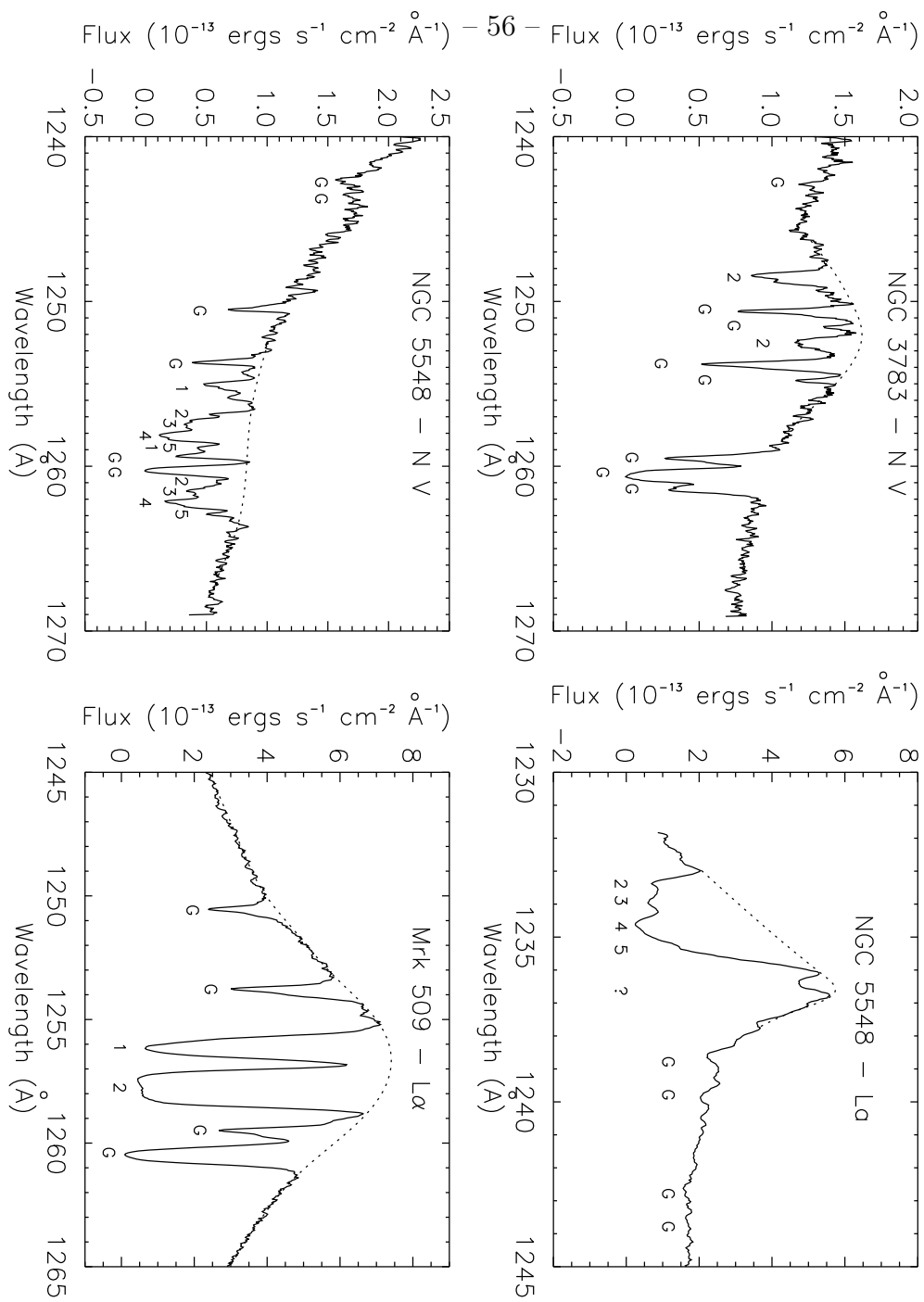


Fig. 4.